

ACTIVATED CARBONS AS ADSORBENTS OF METHYL MERCAPTAN

Svetlana Bashkova, Andrey Bagreev, and Teresa J. Bandosz

Department of Chemistry, the City College of New York and the Graduate School of the City University of New York, 138th street and Convent Ave, New York, NY 10031; e-mail: tbandosz@ccny.cuny.edu

Introduction

An objective of this paper is to describe in detail the adsorption of methyl mercaptan from wet air streams on activated carbons. However, the process has been studied [1-3], to our best knowledge there is no extensive study of this phenomenon. This is due to the low odor threshold for methyl mercaptan and its toxic properties. The purpose of the present work is to make an attempt to identify the reaction products and to study the influence of the carbon surface on the removal/oxidation of methyl mercaptan. The preliminary research clearly shows high (100%) efficiency of methyl mercaptan removal on activated carbons at ambient conditions. Our outgoing research focuses on throwing more light on the mechanism of adsorption/oxidation and on a specific role of various surface features.

Experimental

Materials. Four commercial activated carbons of various origins were used in this study. They are as follows: BAX-1500 (wood based -Westvaco), S208 (coconut shell - Waterlink Barnabey and Sutcliffe), Centaur (catalytic carbon - Calgon), and BPL (bituminous coal - Calgon).

The as received materials were studied as adsorbents for methyl mercaptan in the dynamic tests described below. After this test and purging with air the samples are considered as exhausted and they are designated with an additional letter "E".

Methods. Dynamic tests were carried out at room temperature to evaluate the capacity of the sorbents for CH₃SH removal under wet conditions. Adsorbent samples were ground (1-2 mm particle size) and packed into a glass column (length 370 mm, internal diameter 9 mm, bed volume 6 cm³) and prehumidified with moist air (relative humidity 80 % at 25 °C) for one hour. The amount of water adsorbed was estimated from the increase in the sample weight. Moist air (relative humidity 80 % at 25 °C) containing 0.3 % (3,000 ppm) CH₃SH was then passed through the column of adsorbent at 0.5 L/min. The breakthrough of CH₃SH was monitored using a MicroMax monitoring system (Lumidor) with an electrochemical sensor. The test was stopped at the breakthrough concentration of 50 ppm. The adsorption capacities of each sorbent in terms of mg of CH₃SH per g of carbon were calculated by integration of the area above the breakthrough curves, and from the CH₃SH concentration in the inlet gas, flow rate, breakthrough time, and mass of sorbent. For each sample the CH₃SH test was repeated at least twice. The amount of weakly adsorbed CH₃SH was evaluated by purging the adsorbent column with carrier gas at 0.35 L/min immediately after the breakthrough experiment. The CH₃SH concentration was monitored until it dropped to 1 ppm. The process took about up to 3 hours depending on the type of adsorbent.

Nitrogen adsorption isotherms were measured using an ASAP 2010 analyzer (Micromeritics, Norcross, GA, USA) at -193 °C. Before the experiment the samples were degassed at 120 °C to constant pressure of 10⁻⁵ torr. The isotherms were used to calculate the specific surface area, S_{N2}; micropore volume, V_{mic} and total pore

volume, V_t. All the parameters were determined using Density Functional Theory (DFT) [4].

To evaluate the surface pH a 0.4 g sample of dry adsorbent was added to 20 mL of deionized water and the suspension stirred overnight to reach equilibrium. The sample was filtered and the pH of solution was measured using an Accumet Basic pH meter.

Thermal analysis was carried out using TA Instruments Thermal Analyzer (New Castle, DE, USA). The heating rate was 10 deg/min in a nitrogen atmosphere at 100 mL/min flow rate.

Results and Discussion

The methyl mercaptan breakthrough curves are presented in Figure 1. The methyl mercaptan breakthrough capacities calculated from those experiments are summarized in Table 1 along with the pH values of the carbon surfaces, before and after exhaustion, and the amount of water adsorbed during the prehumidification step. The data collected indicate differences in the performance of carbons. The exceptionally high capacity was found for coconut shell-based carbon, S208. Although the large capacity was also found for Centaur, its performance is still worse than that for S208. There are also differences in the adsorption of methyl mercaptan on wood based and bituminous coal based carbon. For the former the capacity is basically nil and the breakthrough occurred just seconds after the tests started. For the latter material the capacity is similar to that obtained on catalytic carbon, Centaur.

Table 1. pH of the surface, amount of water preadsorbed, and CH₃SH breakthrough capacities for the materials studied.

Sample	pH/pHE	Amount of water	CH ₃ SH capacity [mg/g]	CH ₃ SH desorbed [mg/g]
BAX	7.03/7.00	165.5	0	0
BPL	7.96/6.90	86.1	251	0.04
S208	10.11/10.01	94.3	349	0.07
Centaur	7.30/5.24	93.4	230	0.08

As seen from Table 1, the capacity on Centaur is large, however its pH is close to neutral. On the other hand, the capacity of BAX is nil, in spite of the fact that its average pH is almost equal to that for Centaur. Moreover, the large capacity is reported for BPL carbon whose pH is only slightly higher than that for BAX. Discussing these data we have to take into consideration that the pH reported in Table 1 is the average pH of the carbon surface and the "local" pH inside pores can be different, especially when pores are small and functional groups are present at their entrances [5, 6]. Since in the case of CH₃SH dissociation must be important as for H₂S it is likely that some pH threshold exists and the pH of BAX can be below that value [7]. Another factor, which should be taken into account is the manufacturing technology. The neutral pH of the as received BAX is likely the result of surface neutralization with base after activation with phosphoric acid, which usually results in carbons with acidic pH [8].

Although the pH of carbons decreased after methyl mercaptan adsorption no relationship is found between the amount adsorbed and the variations in pH. The effect on catalytic carbon may suggest that acids are formed on the surface as a result of methyl mercaptan oxidation. Since a decrease in the pH is relatively small compared to hydrogen sulfide oxidation where sulfuric acid was formed [5, 6, 8, 9] it is possible that small amount of sulfur-containing acid along with disulfides, are the products of the surface reaction. For other carbons, even with the large amount adsorbed as in the case of S208, a decrease in pH is very small.

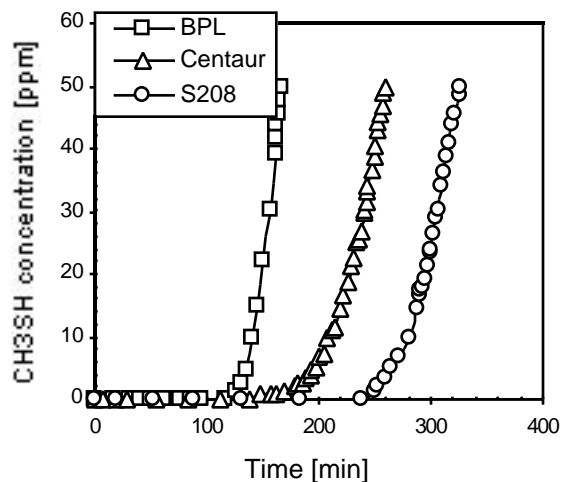


Figure 1. CH₃SH breakthrough curves.

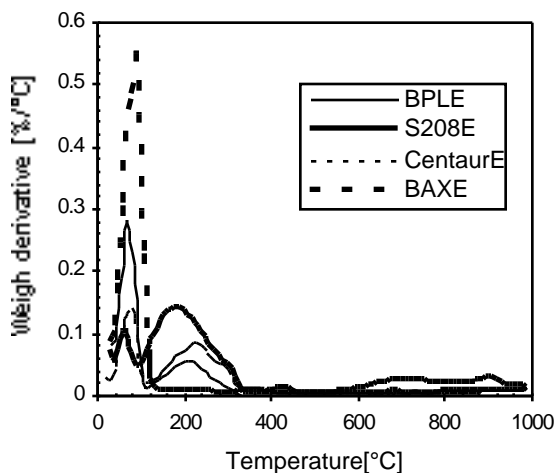


Figure 2. DTG curves in nitrogen for exhausted samples.

The species present on the carbon surface after adsorption can be analyzed using DTG curves obtained in nitrogen. This method was used for the analysis of the products of hydrogen sulfide oxidation [5, 6, 9], sulfur dioxide adsorption [10], and chemisorption of organosulfur compounds on gold [11]. It is assumed that the peak at temperature smaller than 100 °C represents the desorption of weakly adsorbed species (Figure 2) likely water. The peak between 100 and 300 °C might represent desorption of disulfides [11], or removal of methane sulfonic acid relatively weakly adsorbed on the surface. Since methyl mercaptan is expected to be adsorbed very weakly on the surface due to its physicochemical properties (e.a. CH₃SH is desorbed from the gold surface between -83°C and -50 °C [11]), we exclude its presence in the adsorbed phase. For all carbons after exhaustion the two mentioned above peaks are present (Figure 2). The second peaks show the features of heterogeneity of species manifested by the presence of a shoulder around 300 °C with a sharp decrease in the weight loss. This is seen in the most pronounced way for S208 carbon. The shoulder may represent decomposition of surface oxygen complex, CH₃SSCH₃ • n O₂,

which desorbs as SO₂ or SO₃. Oxygen, if present in this form, does not contribute to a decrease in the pH value of the carbon surface after exhaustion. Supporting for this is its temperature of desorption which is close to the temperature of desorption of weakly adsorbed SO₂ or SO₃ on activated carbons [10]. In the case of Centaur, owing to its decrease in the pH after exhaustion, we may expect desorption of small amount of sulfur-containing acid as a ~300 °C shoulder [12]. This peak likely represents sulfur containing acids. This is the effect of nitrogen containing catalytic centers located in small pores as described in the case of hydrogen sulfide adsorption [6].

Another reason for the low capacity of BAX carbon, besides its low pH, may be in its pore structure [13]. BAX and BPL have the highest pore volume, whereas Centaur - the lowest. As expected, the same trend is found in the volumes of micropores and surface areas. The most homogeneous from the point of view of microporosity is S208, whereas BAX is the most heterogeneous sample. The small pores are also present in Centaur. The presence of large pores can affect the sorption capacity of BAX carbon. Even if its pH is favorable for the dissociation of methyl mercaptan in the pore system, which likely enables its oxidation, the pores can be too big to enhance the methyl mercaptan adsorption, especially when preadsorbed water is present (7.7 weight % as indicated from Table 1).

Conclusions

Based on the results presented above, some direct relationship between the surface features and the amount of methyl mercaptan adsorption can be found. Moreover, there is an indication of the competition for adsorption sites between water and dimethyl sulfide. This hypothesis seems to be reasonable if we take into account the lack of disulfide solubility in water. The formation of disulfides is enhanced by the presence of water, as a result of dissociation of methyl mercaptan. Disulfides, when formed, are expected to be stronger adsorbed on the surface of carbon than water. Taking into account their incompatibility with water molecules it is likely that they replace adsorbed water molecules.

Acknowledgement. Acknowledgement is made to the donors of the Petroleum Research Fund, administered by the ACS, for support of this research (Grant # ACS-PRF#35449-AC5)

References

- (1) Katoh, H.; Kuniyoshi, I.; Hirai, M.; Shoda, M. *Appl. Cat. B: Environ.* **1995**, *6*, 255.
- (2) Dalai, A.K.; Tollefson, E.L.; Yang, A.; Sasaoka, E. *Ind. Eng. Chem. Res.* **1997**, *36*, 4726.
- (3) Ishizaki, C; Cookson, I.T. In *Chemistry of Water Supply, Treatment and Distribution*; Rubin, A.I. Ed., p.157, Ann Arbor Science, Ann Arbor, MI, 1981.
- (4) Olivier, J.P. *J. Porous Materials* **1995**, *2*, 9.
- (5) Adib, F.; Bagreev, A.; Bandosz, T.J. *Environ. Sci. Technol.* **2000**, *34*, 686.
- (6) Adib, F.; Bagreev, A.; Bandosz, T.J. *Langmuir* **2000**, *16*, 1980.
- (7) Bagreev, A.; Adib, F.; Bandosz, T.J. *Carbon* **2001**, *39*, 1987.
- (8) Adib, F.; Bagreev, A.; Bandosz, T.J. *J. Coll. Interface Sci.* **1999**, *214*, 407.
- (9) Adib, F.; Bagreev, A.; Bandosz, T.J. *J. Coll. Interface Sci.* **1999**, *216*, 360.
- (10) Bashkova, S.; Bagreev, A.; Bandosz, T. J. *Environ. Sci. Technol.* **2002**, *18*, 1257.
- (11) Nuzzo, R. G.; Zegarski, R. B.; Bubo, L.H. *J. Am. Chem. Soc.* **1987**, *109*, 773.
- (12) Bagreev, A.; Rahman, H.; Bandosz, T.J. *Carbon* **2001**, *39*, 1319.
- (13) Bashkova, A.; Bagreev, A.; Bandosz, T.J. *Environ. Sci. Technol.* In press.

CHARACTERIZATION OF AMBIENT CARBONACEOUS PARTICLES USING ELECTRON MICROSCOPY TECHNIQUES

Gary S. Casuccio, Traci L. Lersch and Steven F. Schlaegle
RJ Lee Group, Inc., 350 Hochberg Road, Monroeville, PA 15146

Donald V. Martello

U. S. Department of Energy, National Energy Technology
Laboratory, PO Box 10940, Pittsburgh, PA 15236

Introduction

The current understanding of the carbonaceous component associated with ambient particulate matter is limited. In most ambient speciation studies, carbon is determined through the thermal/optical evolution analysis of particulate matter collected on quartz fiber filters. Although organic carbon and elemental carbon are determined using the thermal/optical method, there is disagreement as to the accuracy of the results.¹ Furthermore, since organic carbon can originate from both combustion and naturally occurring sources, there is a need to obtain additional resolution on the organic fraction.

In an effort to improve the current understanding of the carbonaceous component associated with fine particulate matter, the U. S. Department of Energy (DOE), National Energy Technology Laboratory (NETL) is conducting studies that are designed to provide greater resolution on the carbonaceous component. As part of this effort, scanning electron microscopy (SEM), computer controlled scanning electron microscopy (CCSEM) and transmission electron microscopy (TEM) techniques are being employed to provide detailed information on individual carbon particle characteristics.

This paper outlines how electron microscopy methods are being used to complement the bulk carbon analysis methods. Information is provided to illustrate how morphology and individual particle chemistry data can be used to help speciate carbonaceous particulate matter.

Experimental Results

Electron microscopy is best performed on particles that are collected as a monolayer on a microscopically smooth filter substrate with minimal particle agglomeration. The polycarbonate (PC) membrane filter, because of its microscopically smooth surface, is a good substrate for the SEM, CCSEM and TEM analyses. Speciation samplers and "mini-vol" samplers are being used in the NETL studies to collect particles on PC filters at flow rates (~7 l/min) that typically produced samples that are well suited for electron microscopy analysis. Gravimetric analysis indicates that the PC filter sample concentrations ($\mu\text{g}/\text{m}^3$) are in close agreement to those collected on Teflon filters using the speciation sampler and also with samples collected with the FRM sampler.²

Preparation for the SEM and CCSEM analyses was performed by removing a wedge shape section (~1/8 the filter) of the filter and securing on a SEM stub using either double sided silver tape, conductive carbon tape or colloidal graphite in butanol ("DAG"). The samples were not coated with carbon or metals to permit examination of the particulate matter similar to the as-collected state. TEM preparation involved coating the sample with a thin layer of

carbon by evaporative deposition under vacuum and dissolving the PC filter in chloroform. This process leaves the particles attached to the thin carbon replica. Volatile particle species (e.g., secondary organic aerosols) may be removed during the TEM preparation.

SEM analyses were performed using the Personal SEM (Aspex Instruments) and JEOL 840 (Japan Electron Optics Laboratory) instruments. Each SEM was equipped with secondary and backscattered electron detectors coupled with an energy dispersive X-ray spectrometer (EDS) system capable of detecting elements with atomic number 6 (carbon) and greater.

The secondary electron (SE) detector yields an image that has excellent sharpness and depth of focus, which results in an image with a three-dimensional perspective. The backscattered electron (BE) detector provides an image that is dependent on the number of backscattered electrons generated when the electron beam interacts with the sample. This interaction results in intensity variations in which features consisting of higher atomic numbered elements appear brighter than features consisting of lighter elements. Thus, the contrasting brightness in a backscattered electron image is a function of composition that is not apparent in the secondary electron image. X-rays are also produced by the interaction of the electron beam and the specimen. The energy of the x-rays depends on the configuration of the electrons in the atoms of the material being examined; that is, it depends upon its elemental composition.

The secondary, backscattered and X-ray signals can be collected in synchronization with the position of the electron beam to provide highly detailed spatial and compositional information of microscopic features. With respect to characterization of carbonaceous particles, the SE and BE electron images combined with micro-chemical analysis provide a resolution that can not be obtained using the traditional bulk analytical techniques. This increased resolution is illustrated in Figure 1. In this figure, SE images and elemental spectra are provided for a carbon chain agglomerate feature and a biological (pollen) feature. The EDS spectrum indicates that the carbon chain agglomerate is composed primarily of carbon with a small amount of sulfur. The pollen is also composed primarily of carbon with small levels of potassium, sulfur and phosphorus. In general, biological material consisting of pollen and spores can be distinguished based on a distinct morphology and trace elements such as potassium and phosphorus.

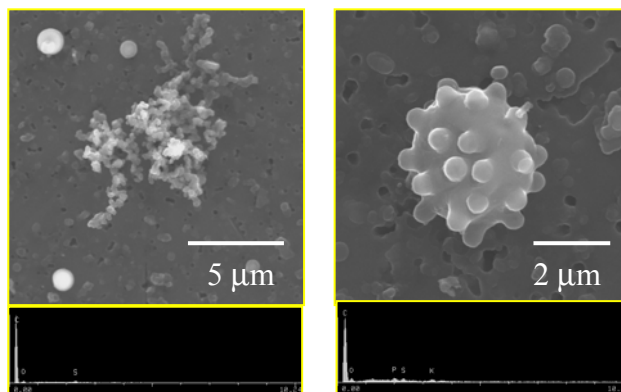


Figure 1. SE image and elemental spectra of a carbon chain agglomerate particle (left) and biological particle (right).

X-ray analysis of the particles at an accelerating voltage of 15kV produces an electron beam penetration on the order of 5 μm for

carbonaceous material. Thus, some of the carbon X-rays can be expected to originate from the PC filter substrate. In an effort to eliminate extraneous carbon X-rays generated from the filter matrix, the PC filters were coated with palladium prior to sample collection. Figure 2 provides SE images and elemental spectra of spherical alumino-silicate (SAS) particles. The image on the left is a SAS particle that was collected on a PC filter. The peak on the far left in the spectrum below the image is carbon. The image on the right is also a SAS particle. This particle was collected on a palladium coated PC filter. Note that carbon was not detected in this particle indicating that the carbon measured from the SAS particle on the left was generated from the filter matrix. The ability to effectively eliminate carbon X-rays from the filter matrix enables a better estimate on the carbon component.

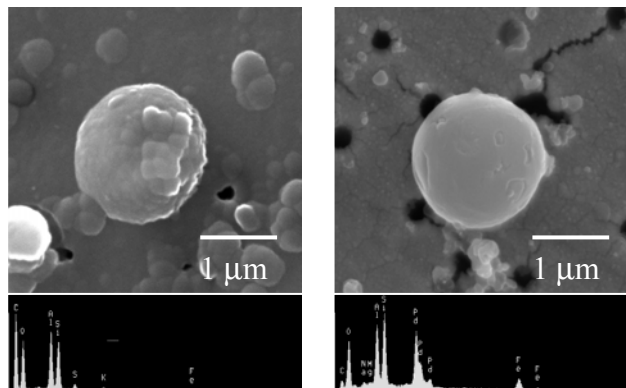


Figure 2. SE images and elemental spectra of SAS particles collected on a PC filter (left) and a palladium coated PC filter (right).

Although the manual SEM analysis can be used to provide a wealth of information on the characteristics of individual particles, quantitative data on particle concentrations and distributions is limited with this technique. This is due to the number of particles that can be analyzed effectively from the perspective of time and cost. CCSEM overcomes this limitation because it permits sufficient numbers of particles to be analyzed in an efficient manner ensuring representation of the particle population.³ With CCSEM, the size, shape (aspect ratio) and elemental composition associated with individual particles are measured and recorded in a totally automated fashion. A digital image can also be recorded for each particle (or a subset of particles) during the analysis. The CCSEM data can be summarized and reviewed off-line to potentially provide additional information based on the manual examination of the data.⁴ Thus, CCSEM analysis provides the ability to merge the strengths of a automated analysis with those obtained from a manual SEM analysis.

To evaluate whether the CCSEM carbon results were comparable to those obtained using other carbon analytical methods, an evaluation was performed on a set of seven samples. The CCSEM carbon data was obtained from samples collected on palladium coated PC filters. The CCSEM results were compared to carbon data collected using an Rupprecht & Patashnick (R&P) 5400 Ambient Carbon Particulate Monitor. Figure 3 provides a comparison of the CCSEM and R&P carbon results.

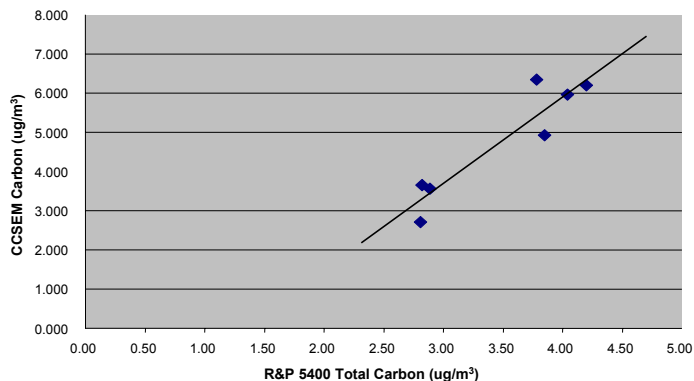


Figure 3. Comparison of CCSEM and R&P 5400 carbon data. ($\mu\text{g}/\text{m}^3$).

Results show fairly good agreement suggesting the CCSEM carbon data can be considered quantitative. Off-line review of the carbon particle images is currently being performed to further classify the carbon into subtypes consisting of pollen/spores, vegetative detritus, other biological, and soot/combustion products.

To provide additional information on the fine particle component, TEM analysis are also being employed. The TEM not only offers increased resolution for identification of submicron particles, it has the ability to provide information on molecular structure of crystalline structures through measurement of selected area electron diffraction analysis (SAED) patterns. Figure 4 provides a TEM image of $\text{PM}_{2.5}$ particles and an electron diffraction pattern of an ammonium sulfate particle.

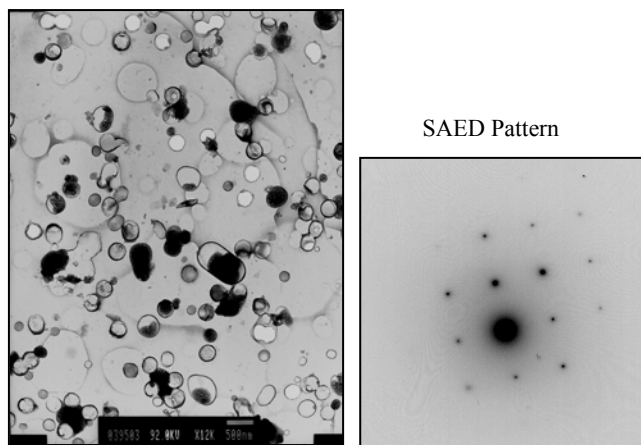


Figure 4. TEM micrograph and SAED pattern of an ammonium sulfate particle.

With respect to carbon, the TEM is being employed to provide additional resolution on carbon chain agglomerate (CCA) structures. The CCA features are a by-product of oil based fuels and thus can be used as an indicator of vehicular emissions. As part of this effort, the TEM carbon data is being compared to the elemental carbon results obtained using the thermal/optical evolution analysis method. The TEM analyses are being performed using JEOL 1200 and JEOL 2000 instruments. Each TEM is equipped with an energy dispersive X-ray spectrometer (EDS) system capable of detecting elements with atomic number 11 (sodium) and greater. The analysis protocol involves manual identification, counting, and measurement of the carbon chain agglomerates. The carbon chain agglomerates are

identified based on their unique morphological characteristics. The TEM data is used to estimate the mass of the carbon chain particles on the filter. This information is then compared directly to the elemental carbon data obtained using the thermal/optical method. Figure 5 provides TEM images of carbon chain agglomerate structures. Note the unique morphology associated with these particles.

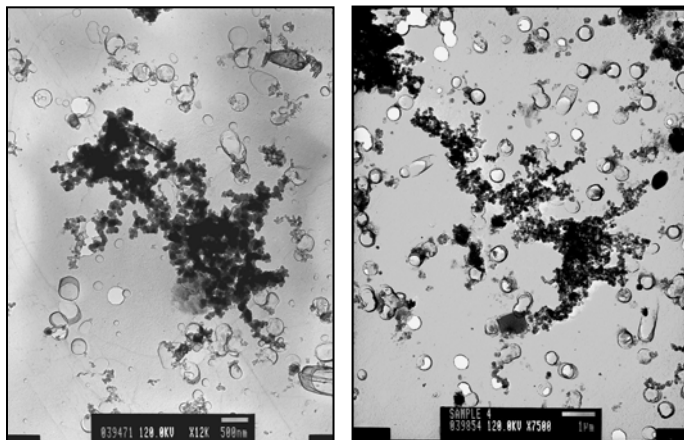


Figure 5. TEM images of carbon chain agglomerated particles.

Current efforts are focused on examining samples collected in a rural location (Holbrook, Greene County, PA) to samples collected in the Lawrenceville section of Pittsburgh, PA. Four 6-hour filter samples were collected at the Lawrenceville site and one 24-hour sample was collected in Holbrook over the same time period. Initial examination of the samples using TEM show higher concentrations of CCA on the Lawrenceville samples. This is illustrated in Figure 6.

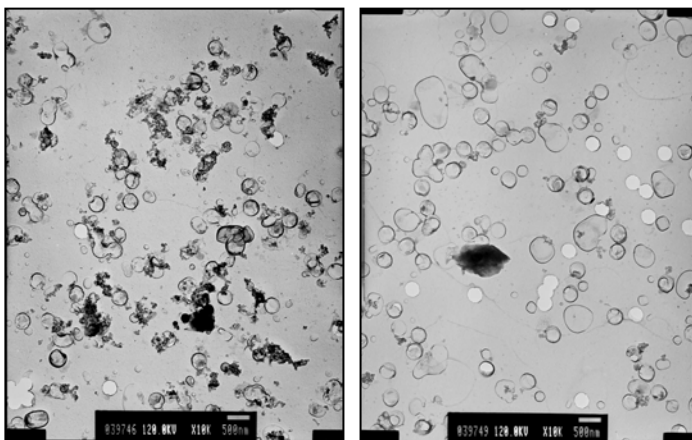


Figure 6. TEM image of samples collected in urban Lawrenceville (left) and rural Holbrook (right). The Lawrenceville sample contains a greater number of CCA particles.

TEM analysis for CCA particles was performed on the four samples collected over 6-hour periods at Lawrenceville on August 12, 1999. TEM CCA results varied from 6.2 percent (0000-0600 hours) to 28.6 percent (1800-2400 hours). The results from the Holbrook sample collected over a 24-hour period were significantly lower (3.8 percent). The TEM CCA values were compared to the elemental carbon (EC) results obtained from the analysis of samples collected on the same date using the thermal/optical technique. The

TEM CCA and thermal/optical EC results are summarized in Table 1. Comparison of the CCA and EC results shows fairly good agreement on four of the samples. A significant difference in the CCA and EC results was reported for the Lawrenceville, (18000-2400) sample. These results suggest that the EC component is composed of CCA. The results also indicate that there are significant differences between the urban and rural sites for CCA particles. Assuming that the majority of the CCA originate from vehicular emissions, the TEM results indicate that the impact from vehicular emissions was significantly higher at the urban site on this day.

Table 1. Comparison of TEM carbon chain agglomerate particles results and EC results for samples collected on August 12, 1999.

Location	Collection Time	TEM CCA Wt. %	EC Wt. %
Lawrenceville	0000-0600	6.2	10.1
Lawrenceville	0600-1200	27.1	20.0
Lawrenceville	1200-1800	14.5	11.1
Lawrenceville	1800-2400	28.6	10.5
Holbrook	0000-2400	3.8	3.4

Summary

SEM, CCSEM and TEM are capable of providing additional resolution on the ambient carbon component. Since bulk analysis methods indicate that approximately 1/3 of the total particle mass on ambient samples could be composed of carbon particles, there is both the interest and need to provide additional information on the characteristics and sources of this component. Effective utilization of electron microscopy techniques with bulk analytical methods offers the potential to provide greater insight on the concentrations and sources of organic and elemental carbon species.

Acknowledgement. The authors would like to acknowledge the assistance of Robinson Khosah and Terry McManus of Advanced Technology Systems, Inc.

Disclaimer

Reference in this report to any specific commercial product, process, or service is to facilitate understanding and does not necessarily imply its endorsement or favoring by the United States Department of Energy.

References

1. Chow, J.C., Watson, J.G., et al., "Comparison of IMPROVE and NIOSH Carbon Measurements," *Aerosol Science and Technology*, **34**: 23-34 (2001).
2. Martello, D.M., Anderson, R.R., et al., "Quantitative Scanning Electron Microscopy Methods to Characterize Ambient Air PM_{2.5}, American Chemical Society, Fuel Chemistry Division Preprints, 2001, 46(1).
3. Casuccio, G.S., Janocko, P.B., et al., "The Use of Scanning Electron Microscopy in Environmental Studies," *J. of Air Poll. Control. Assoc.*, **33**, No. 10, pp. 937-948, October 1983.
4. Henderson, B.C., Stewart, I.M., Casuccio, G.S., "Rapid Acquisition/Storage of Electron Microscope Images," *American Laboratory*, pp. 49-52, November 1989.

Characterization of PM_{2.5} Chemical Composition in the Ambient Air of Beijing, China

Fumo Yang^a, Kebin He^{a*}, Yongliang Ma^a, Qiang Zhang^a, Steven Cadle^b, Tai Chan^b, Patricia Mulawa^b, Chak K. Chan^c, Xiaohong Yao^c

^aDepartment of Environmental Science and Engineering
Tsinghua University, Beijing 100084, PRC

^bGM Research & Development
480-106-269, Warren, MI, 48090-9055, USA

^cDepartment of Chemical Engineering, The Hong Kong University of Science & Technology, Clear Water Bay, Hong Kong, PRC

Introduction

Rapid development and dense population have exacerbated air pollution problems in China's medium and large cities. In response, China is intensifying its air pollution abatement efforts. Since October 1998, Beijing has initiated clean air programs due to mounting public and official concern about the capital's poor air quality. While gaseous pollutants such as sulfur dioxide, carbon monoxide, and oxides of nitrogen (NO_x) have been effectively reduced, the concentrations of PM are still high in Beijing. PM_{2.5} is not monitored routinely in urban areas and there are sparse researches on it till now. As a result, relatively little is known about the status and trends of fine particle mass and composition over time in these areas. However, there is substantial concern about the visibility deterioration in Beijing since it is highly correlated with PM_{2.5}.

Weekly PM_{2.5} measurements were made continuously at two sampling sites for over one year starting in July 1999 with the goal of establishing a comprehensive database to describe fine particulate pollution in Beijing. Mass, ions, carbon, and 40 elements were measured. This paper will summarize the major findings for mass and composition of PM_{2.5} in Beijing with a focus on the seasonal variations of the major components.

Experimental

One week integrated PM_{2.5} samples on filters were taken simultaneously at two sites in Beijing: one located downtown at an air quality monitoring station in Chegongzhuang, and one on the campus of Tsinghua University in a residential area (Figure 1). The Chegongzhuang site lies between the western 2nd and 3rd ring roads, both artery roads in the urban area with busy traffic. The Tsinghua site lies outside of the northern 4th ring road also with busy traffic. Around the site, many residents still use small coal-burned ovens for cooking and heating. The distance between the two sites is 10 km.

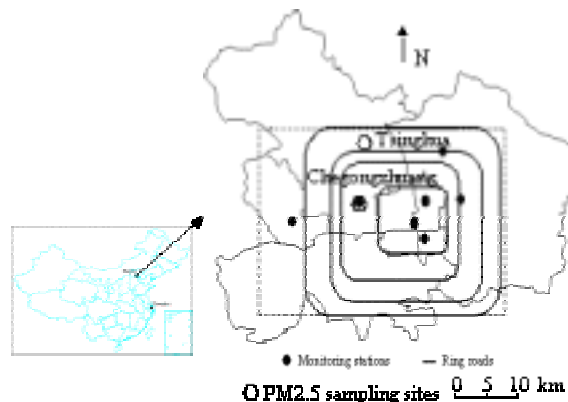


Figure 1. Beijing airshed and location of the sampling sites.

A low-flow rate sampler was deployed at each of the two sites to collect airborne PM_{2.5}. At each site, the sampler was placed on the roof of a 3m-tall building, resulting in an effective inlet height above the ground of about 4.5m. The sampler is a chemical speciation one for PM_{2.5}, which was designed to minimize sampling artifacts for nitrate via a carbonate solution coated denuder followed by a Nylon filter. It runs at a flow rate of 0.4 l/min with a sampling duration of one week. X-ray fluorescence (XRF), ion chromatography (IC), and thermal/optical reflectance (TOR) were employed to analyze 40 elements (from Na to U), water-soluble ions, and organic and elemental carbon (OC and EC), respectively. Sampling system, chemical analysis, and quality control for this study has been introduced elsewhere¹.

Results and Discussion

Weekly PM_{2.5} concentrations ranged from 37 to 357 $\mu\text{g}\cdot\text{m}^{-3}$ with annual mean of 115 and 127 $\mu\text{g}\cdot\text{m}^{-3}$ in 2000 at the Chegongzhuang and Tsinghua sites, respectively. PM_{2.5} concentrations were highest during the winter, decreased through the spring, and tended to be lowest during late spring, summer, and early autumn. There were similar weekly and seasonal trends in PM_{2.5} concentrations for the two sites, and modest differences were found for the PM_{2.5} concentrations between the two sites during most of sampling periods. Given the similarity in the data, it appears that the proximity of the downtown site to the second ring road was not a major factor. As diagrammed in Figure 2, the three fractions of particles usually varied similarly from week to week, while PM₁₀ varied more consistently with TSP (total suspended particles, referred to particulate matter with aerodynamic diameters less than 100 μm in China) than PM_{2.5}. PM_{2.5} constituted 55% PM₁₀ and 29% of TSP on one year basis, with PM_{2.5} to PM₁₀ and TSP ratios varying from season to season. Fine particles dominated PM₁₀ in the fall and winter, with PM_{2.5} fraction amounting to 59% and 66%, respectively, while it was 42% and 49% in the spring and summer, respectively. Both PM_{2.5} to PM₁₀ and TSP ratios peaked in winter and were lowest in spring, suggesting substantially increased heating sources in winter contributed more to fine particles, while frequently occurred dust storms in spring did more to coarse particles.

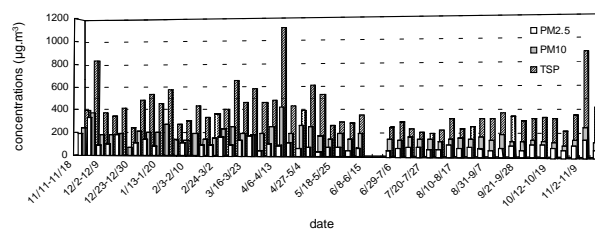


Figure 2. Variations of PM_{2.5}, PM₁₀, and TSP concentrations with time between 11 September 1999 and 16 September 2000 at the Chegongzhuang site.

The most abundant species (generally $>1 \mu\text{g}\cdot\text{m}^{-3}$) were OC, EC, sulfate, nitrate, ammonium, potassium, silicon, calcium, and iron. Of these species, carbon and ions accounted for over half of the measured mass. Soil related crustal species (Al, Si, K, Ca, Ti, Fe, and Zn), without counting their oxides, account for about 8% of the mass. Further investigation on PM_{2.5} speciation at the two sites showed PM_{2.5} compositions were similar between the two sites with divergence coefficient² $CD=0.064$.

Carbonaceous PM represented a significant fraction of PM_{2.5} at the two sites. OC was the most abundant species in PM_{2.5}, constituting more than 20%, and total carbon (also termed

carbonaceous aerosol, is the sum of the OC and EC) averaged 31% of PM_{2.5} mass at the two sites. At the Chegongzhuang site, OC and EC seasonal patterns (**Figure 3**) were similar to those for PM_{2.5}, i.e., the highest concentration occurred in winter and the lowest in summer. The winter average values of OC and EC concentrations were 135% and 77% higher than their summer averages, respectively. On the other hand, OC/EC seasonal ratios were much stable, averaging 2.6-3.0, with annual mean amounting to 2.9. As shown in **Figure 3**, the OC and EC values were highly correlated, suggesting that EC is present along with OC. There were similar results at the Tsinghua site.

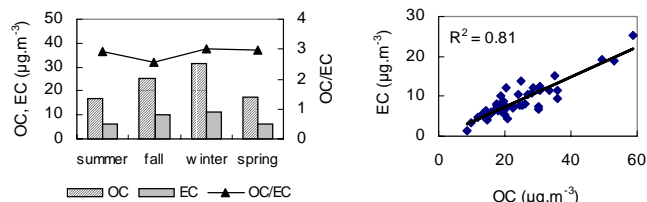


Figure 3. Seasonal variations and correlations of OC and EC concentrations at the Chegongzhuang site.

Sulfate, nitrate, and ammonium in PM_{2.5} are primarily secondary particles, with their abundances mainly determined by their precursor gases concentrations and transformation rates. The sum of the ammonium, nitrate, and sulfate ions accounted for 37% of the seasonal average PM_{2.5} mass in summer, and for about 25% in three other seasons, implying secondary particles were most abundant in PM_{2.5} in urban area of Beijing. As shown in **Figure 4**, seasonal variations of sulfate were quite different from that of SO₂ gas. Contrary to the seasonal patterns of SO₂ gas, summer average of sulfate was much higher than those in the spring and autumn. The seasonal fractions of sulfate to total sulfur ($[\text{SO}_4^{2-}]/([\text{SO}_2] + [\text{SO}_4^{2-}])$) were the following: summer (56%) > autumn (31%) > spring (21%) > winter (11%). The highest value was during the summer, suggesting that SO₂-to-sulfate transformation rates peaked in the summer due to enhanced summertime photochemical oxidation and SO₂ oxidation in clouds. On the other hand, the abundance of sulfate in winter could be related to high concentrations of SO₂, which are likely due to increased coal consumption during heating period combined with poor dispersion. The sulfate versus total sulfur gave a summer average ratio of 3, implying that nearly all of the PM_{2.5} sulfur was present as sulfate in this season.

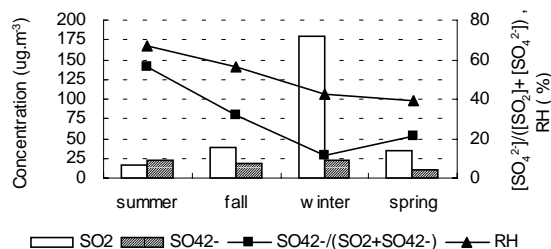


Figure 4. Seasonal patterns of sulfate in PM_{2.5}, SO₂, sulfate to total sulfur ratios, and relative humidity at the Chegongzhuang site.

At the Chegongzhuang site, nitrate concentrations exhibited strong fluctuation on a seasonal basis (**Figure 5**), with the seasonal mean concentrations proceeding in the following manner: winter > spring > summer, which were similar to the seasonal patterns of PM_{2.5} mass. The highest is 13.2 µg/m³ in winter and lowest 5.5 µg/m³ in summer, with a factor of 2.4 difference. Note that NO_x

concentrations only had a factor of near 2 difference for the same periods. This could be related to the low temperature (<15 °C) in late fall and winter that favors a shift from the gas phase as nitric acid to the particle phase as ammonium nitrate, and that most nitrate will be in the gas phase at temperature greater than 30 °C³. The amount of nitrate present on the backup nylon filters was 47, 23, 19, and 20% for the summer through spring, respectively. This nitrate is due to the volatilization of ammonium nitrate from the front Teflon filter.

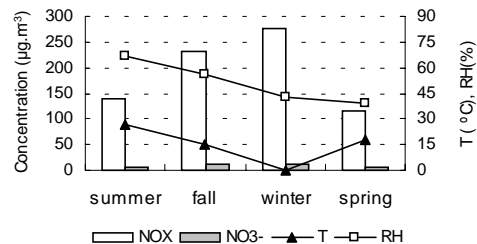


Figure 5. Seasonal patterns of nitrate in PM_{2.5}, NO_x, temperature, and relative humidity at the Chegongzhuang site.

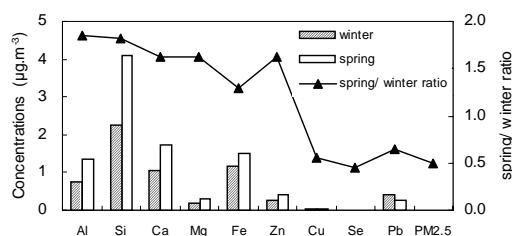


Figure 6. Comparison of crustal-related and trace elements between winter and spring at the Chegongzhuang site.

Figure 6 gives a comparison of the main crustal-related elements and some trace elements at the Chegongzhuang site between the winter and spring. In contrast to the PM_{2.5} mass decreasing sharply from the peak in the winter to a much lower value in the spring, concentrations of crustal species such as aluminum, silicon, calcium, magnesium, and iron elevated sharply from winter to spring and peaked then. The spring to winter average concentration ratios for these species were 1.3-1.9, while those for PM_{2.5} and several trace elements such as copper, selenium, and lead, which arise mainly from anthropogenic sources, were about 0.5. It probably implied frequent dust storms had much more impact on crustal-related elements than trace elements during the spring of 2000 when twelve major dust storms swept Beijing, the worst frequency and severity in 50 years. The weekly peak of silicon (16.2 µg·m⁻³) during the spring exceeded the winter value by a factor of 3.6, which also reflected the impact of dust storms.

Acknowledgment

This work was supported by GM Research and Development Centers.

References

- He, K.; Yang, F.; Ma, Y.; Zhang, Q.; Yao, X.; Chan, K. C.; Cadle, S.; Chan, T.; Mulawa, P., *Atmospheric Environment*. 2001. 35: 4959-4970
- Zhang, Z.; Friedlander, S. K., *Environmental Science & Technology*. 2000. 34: 4687-4694.
- US EPA. Particulate matter (PM_{2.5}) speciation guidance document. 1999

CHARACTERIZATION OF PM_{2.5} FROM RURAL MIDWESTERN U.S. SITES

C.R. Crocker, K.E. Eylands, D.P. McCollor, B.S. Helmowski, S.A. Benson, and K.C. Galbreath

Energy & Environmental Research Center
University of North Dakota
Box 9018
Grand Forks, ND 58202-9018

Introduction

Most studies involving the characterization of fine particulate matter (PM_{2.5}) have focused on samples collected from industrialized or urban environments probably because outdoor air quality is generally poorer in such environments. Rural areas in the upper midwestern United States do not experience the serious atmospheric pollution problems generally encountered in large urban settings. Even though upper midwestern states are in compliance with national and state ambient air quality standards for PM_{2.5} (1, 2), concerns exist about potential respiratory health risks associated with the releases of PM_{2.5} (3).

The purpose of this study is to sample and characterize PM_{2.5} and apportion the particles to possible sources based on point source dispersion modeling and prevailing wind direction. PM_{2.5} samples were collected from three rural locations in the upper midwestern United States and analyzed using an automated scanning electron microscope (ASEM).

Experimental

Fine PM Sampling. Ambient PM_{2.5} samples were collected using a Rupprecht & Patashnick automatic cartridge collection unit (ACCU) attached to a tapered element oscillating microbalance (TEOM Model 1400a). PM_{2.5} was collected on 0.4- μ m-pore-size, carbon-coated, polycarbonate membranes. Precoating of the membranes enabled the direct introduction of PM_{2.5} samples into a scanning electron microscope (SEM) for morphological and chemical analyses. A weather station was used to monitor local meteorological conditions. The ACCU sampled outdoor ambient air under atmospheric conditions continuously for 18 to 31 days loading membranes in 2- to 4.5-day increments depending on total mass collected by the TEOM.

PM_{2.5} emission point sources and ACCU sampling sites are indicated in Figure 1. Sampling at the easternmost site (Site 3) was performed during a period of spring tillage and planting (May 18 – June 15, 2000). This site is remote from large population centers, industrial activity, and thermal power plants. The westernmost site (Site 1) is similarly in an agricultural region, with sampling performed in late summer (August 8–25, 2000) during a period of small grain harvesting. This site is remote from large population centers and industrial activity; however, several large (500-MW_e) coal-fired power plants and a large coal gasification facility are within 110–150 km of the site. Land use in the central southernmost site (Site 2) is dominated by ranching. A well-traveled paved road and an infrequently-traveled gravel road exist within approximately 60 m of the sampling site. Sampling at this site was performed August 27 – September 14, 2001. An oil refinery and several coal-fired power plants are located approximately 95 km west of Site 2. Potential sources of PM_{2.5} at the sampling sites include diesel- and gasoline-fueled motor vehicles, fugitive dust from gravel roads and agriculture, vegetation and fires, an oil refinery, and coal-fired power plants.

ASEM Characterization. ASEM methods, energy-dispersive spectrometry, and digital image analysis techniques were used to determine the size and chemical composition of several thousand particles per sample. Particles $\geq 0.5 \mu$ m in diameter were chemically analyzed. An x-ray spectral matching technique, involving a database of spectra for inorganic compounds, was used to assign each particle composition to a chemical classification. The spectra were also processed to determine elemental concentrations. Along with the size and chemical information from each particle, other information, including particle area, perimeter, maximum diameter, minimum diameter, mean diameter, circularity, and particle location, were recorded.

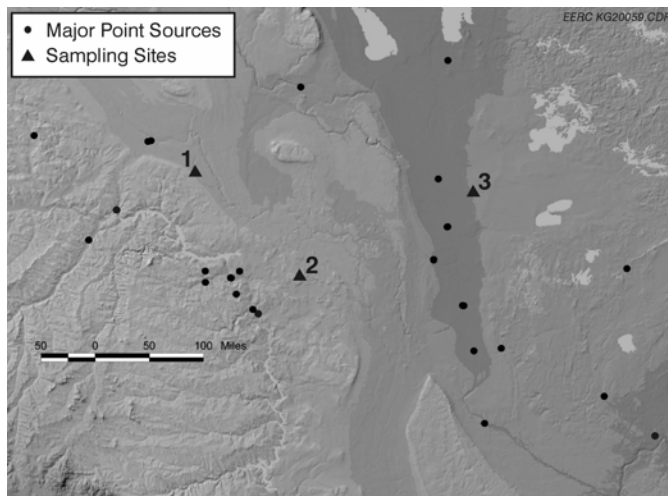


Figure 1. Map of PM_{2.5} Sampling Locations and Major Point Sources

Data Analysis. The particle chemical compositions (C, N, O, Na, Mg, Al, Si, P, S, Cl, K, Ca, Ti, and Fe) were classified into chemical and mineral groups. Eight major chemical categories were identified and used to classify PM_{2.5}. These are quartz, feldspar, clays (e.g., kaolinite, chlorite, muscovite, biotite, and illite), Na–K salts (i.e., NaCl and KCl), carbonates (i.e., calcite, dolomite, ankerite, siderite), iron-rich (e.g., pyrite, magnetite, ilmenite, and hematite), sulfur-rich (e.g., anhydrite and gypsum), and unclassified, which generally consists of chemically complex particles such as mixed clays, clay-coated mineral grains, and/or organic compounds.

Results and Discussion

Dispersion modeling results indicate that the prevailing westerly and northwesterly winds during the sampling campaigns may have contributed primary and secondary combustion PM_{2.5} to the samples collected at Sites 1 and 2. PM_{2.5} collected on the membrane filters generally ranged from <0.4 to 1μ m in diameter. As indicated in Figures 2–4, 79% to 87% of the PM_{2.5} consists of unclassified and organic components. The particles in these classification categories are mostly spores, pollen, soil, and fugitive dust. The remaining 13% to 21% of PM_{2.5} collected at the sites is inorganic rich. The clays, quartz, carbonates, and feldspars are primarily associated with fugitive dust from nearby gravel roads and fields. The alkali salt contents of all three samples are very consistent, suggesting a regional and perhaps natural source for this particle type. PM_{2.5} samples from Sites 1 and 3 are compositionally similar. PM_{2.5} from Site 2, however, contains a greater proportion of sulfur-rich particles, presumably composed of secondary sulfate compounds.

Conclusions

Future work will focus on further characterization of unclassified particles through multivariate cluster analysis and incorporating morphological characteristics into the cluster analysis. Particles may have similar chemical compositions but come from different sources. For example, fly ash and dust from gravel roads are aluminosilicate rich. They are chemically similar but vary greatly by size and shape. Shape factors are being incorporated into ASEM and cluster analysis to distinguish between these particles types.

Acknowledgment. This work was sponsored by the United States Department of Energy under Cooperative Agreement DE-FC26-98FT40320.

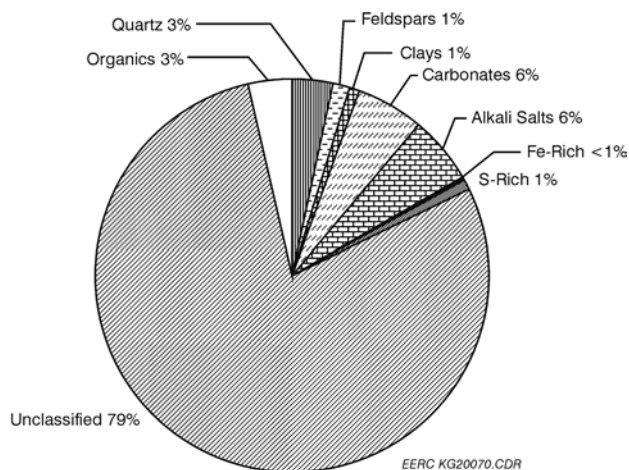


Figure 2. Chemical classification of PM_{2.5} from Site 3.

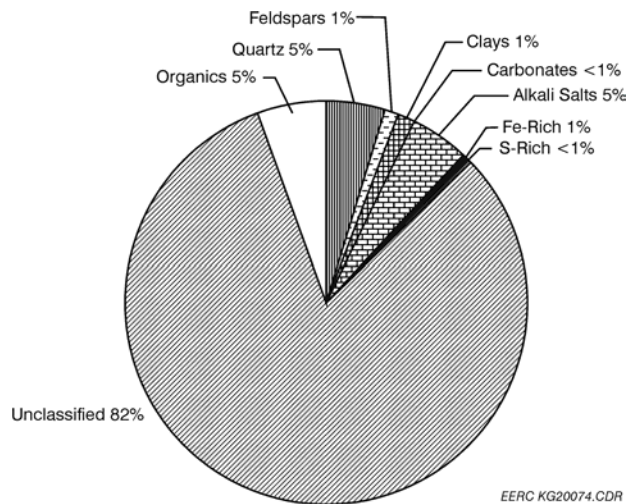


Figure 3. Chemical classification of PM_{2.5} from Site 1.

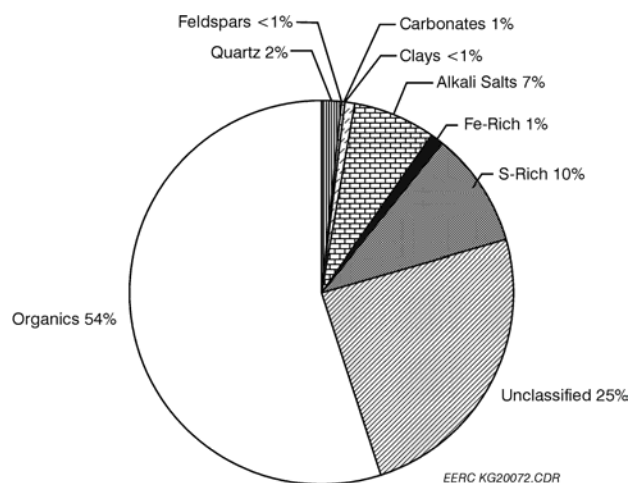


Figure 4. Chemical classification of PM_{2.5} from Site 2.

References

- (1) *Annual Report of North Dakota Air Quality Monitoring Data*; North Dakota Department of Health Division of Air Quality, Sept 2001.
- (2) *Air Quality in Minnesota: Problems and Approaches*; Minnesota Pollution Control Agency, Jan 2001.
- (3) *North Dakota Children's Health Study*; Final Report for North Dakota Department of Health and Industrial Commission of North Dakota by Environmental Health and Engineering, Inc., and Johns Hopkins Bloomberg School of Public Health, Nov 15, 2001.

COMBINING A LEACHING PROCEDURE AND XAFS SPECTROSCOPY FOR IDENTIFICATION OF SULFUR AND METAL SPECIES IN FINE PARTICULATE MATTER FROM COMBUSTION SOURCES

F. E. Huggins, D. Panjala, S. Pattanaik and G. P. Huffman

University of Kentucky, Lexington, KY 40506

J. R. Kyger and J. D. Robertson

University of Missouri, Columbia, MO 65211

W. P. Linak and C. A. Miller

U.S. EPA NRMRL, Triangle Park, NC 27711

Introduction

There is a great need to identify specific elemental compounds in ambient particulate matter (PM) and in closely related particulate matter emitted by both stationary and mobile fossil-fuel combustion sources. Such information, particularly for sulfur and heavy metals, can aid epidemiological studies aimed at discovering the underlying causes of adverse health effects arising from inhalation of airborne PM (1). In addition, specific chemical compounds might be useful as markers for identifying and quantifying different source contributions of PM to ambient PM. In this work, we describe results obtained on the speciation of sulfur and various metals in PM derived from combustion of residual oil and coal using a methodology based on both leaching behavior and X-ray absorption fine structure (XAFS) spectroscopy.

The data presented here augment and update various preliminary accounts of the speciation in suites of coarse ($>2.5 \mu\text{m}$, $\text{PM}_{2.5+}$) and fine ($<2.5 \mu\text{m}$, $\text{PM}_{2.5}$) PM samples based on XAFS spectroscopy alone (2-4). Such previous studies have been conducted largely on as-received PM samples collected and prepared at the EPA's National Risk Management Research Laboratory (NRMRL). The combustion experiments have been described in detail elsewhere (5,6). The coarse and fine fractions of PM were separated by means of a cyclone.

Experimental

Leaching Experiments. Aliquots of fine and coarse PM fractions from combustion of a Baseline #5 (BL5) residual oil and a Pittsburgh-seam (PITT) coal were leached in distilled water, in 1N HCl acid and, for the residual oil samples only, in pentane. Leaching treatments consisted of exposure of the PM sample to a solution for a period of 10-15 minutes while being sonicated at room temperature. Such treatments were repeated five times on each PM sample with fresh solution. The final residues from the leaching experiments were separated from the leaching solutions by filtration and dried overnight in an oven at 60°C . The leachant solutions were combined and saved. Sulfur and metal concentrations in both the residues and the liquid solutions were determined by X-ray fluorescence (XRF) and ICP-MS, respectively.

XAFS Spectroscopy. XAFS spectroscopy was performed for various elements on all solid residues either at beam-lines X-18B and X-19A at the National Synchrotron Light Source (NSLS), Brookhaven National Laboratory, NY, or at beam-line IV-3 at the Stanford Synchrotron Radiation Laboratory (SSRL), Stanford University, CA. XAFS spectra of most metals were determined by

using a 12 or 13 element Ge detector gated to record predominantly the X-rays fluoresced by the element of interest. Sulfur XANES spectra were recorded in fluorescence geometry using a PIPS detector at beam-line X-19A at NSLS. Data reduction and analysis was carried out at the University of Kentucky using standard procedures that are well described in the literature (7).

Results and Discussion

Sulfur. As indicated in Figure 1, the sulfur XANES spectrum of the BL5 $\text{PM}_{2.5+}$ sample exhibits significant changes as a result of the aqueous leaching treatment. Virtually identical changes are also observed for the fine $\text{PM}_{2.5}$ fraction and as a result of acid (HCl) leaching. It is clear from the sulfur XANES that almost all of the sulfate sulfur is leached from both BL5 PM samples in these treatments, leaving thiophenic sulfur, elemental sulfur and inorganic sulfide sulfur as major sulfur forms in the residues. Pentane leaching has only a minor effect on the speciation of sulfur, resulting in a slight reduction in sulfate.

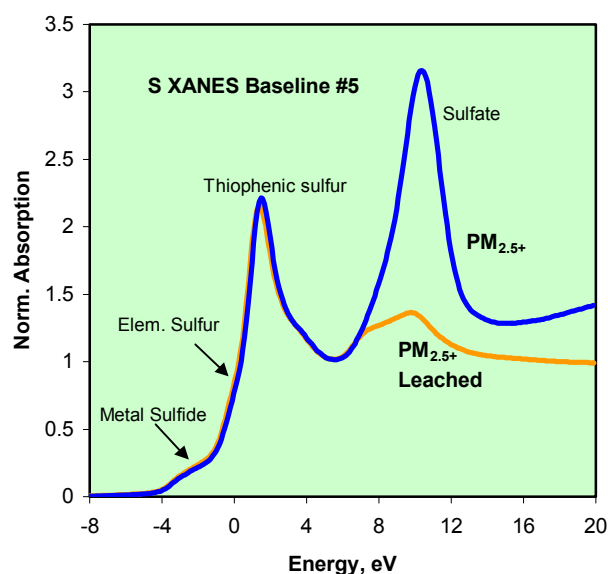


Figure 1. Sulfur XANES spectra of the BL5 $\text{PM}_{2.5+}$ fraction before and after aqueous leaching. Note the close correspondence of the two curves for the less-oxidized forms of sulfur.

The Pittsburgh coal PM fractions exhibit similar behavior with respect to leaching, except that the sulfate is removed in stages with significantly more sulfur being removed during the acidic leach than during the aqueous leach. In similar fashion as to what was observed for the residual-oil PM samples, the less-oxidized forms of sulfur in the coal PM samples do not appear to be significantly altered by either leaching treatment.

The acid treatments also result in increases in chlorine content for the leached residues compared to the unleached material. This was observed for both types of PM.

Metals. Leaching of the coal and residual oil-derived coarse and fine PM samples by aqueous or acid solutions effects significant changes in the XANES spectra of most metals. In particular, the spectra of elements that are present predominantly as sulfates in the PM derived from residual oil exhibit great changes as these sulfates are readily leached by both the aqueous and acidic solutions. Figure 2 shows the Ni XANES spectra of the BL5 $\text{PM}_{2.5+}$ and $\text{PM}_{2.5}$ samples

after pentane and acid leaching. The pentane leaching process has little effect on the nickel XANES spectra and the spectra after pentane leaching are closely similar to the original spectra shown elsewhere (2,4). The spectrum from the acid-leached $PM_{2.5+}$ residue is identified as arising from a nickel sulfide or mixture of sulfides, whereas the spectrum of the acid-leached $PM_{2.5}$ residue is identified as arising predominantly from nickel ferrite ($NiFe_2O_4$). Such observations confirm inferences made from least-squares fitting of the XAFS data for the original, as-received PM sample (4). In addition, we see evidence for a minor sulfide contribution, indicated by the arrow in Figure 2, in the $PM_{2.5}$ residue of acid leaching. Such a contribution was below detection in our earlier spectral work on the as-received samples and is only brought out by removal of the dominant nickel sulfate.

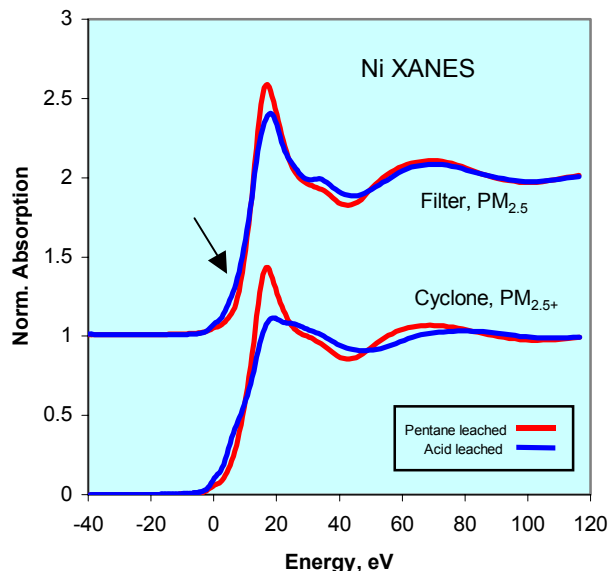


Figure 2. Nickel XANES spectra of the BL5 $PM_{2.5+}$ and $PM_{2.5}$ residue fractions after leachings in pentane and hydrochloric acid. Note the excess absorption indicated by the arrow for the acid-leached $PM_{2.5}$ residue compared to the pentane-leached residue.

One element that appears to exhibit much less change in its spectra as a result of leaching of the residual oil PM samples is iron. As shown in Figure 3, aqueous leaching results in only very minor spectral changes for the $PM_{2.5}$, while the leaching in 1N HCl is more effective. Even less spectral changes are observed for the leaching sequence on the $PM_{2.5+}$ fractions. Such differences between iron and nickel are also apparent from relative changes in concentration as a result of leaching. For example, whereas aqueous leaching induces a reduction in Ni content for the BL5 $PM_{2.5+}$ sample from 3,350 ppm to 900 ppm, the corresponding change in iron content is only from 2,200 ppm to 2,025 ppm. For this particular sample, it would appear that relatively little of the iron is bound up in the form of sulfate; instead, much of the iron is present in oxide form. We have already noted the presence of significant nickel ferrite in the $PM_{2.5}$ sample that could account for much of the iron in oxide form. Again, leaching of the $PM_{2.5}$ fraction does indicate the presence of a very minor fraction of iron sulfide that was not apparent in previous investigations on the as-received material only.

Vanadium, zinc and copper exhibit behavior similar to nickel and show significant reduction as a result of aqueous leaching of the residual oil PM samples. It is clear that these elements contain

readily solubilized species, presumably sulfates, in abundance. Arsenic was completely removed from the residual-oil PM samples by acidic leaching, but not by aqueous leaching.

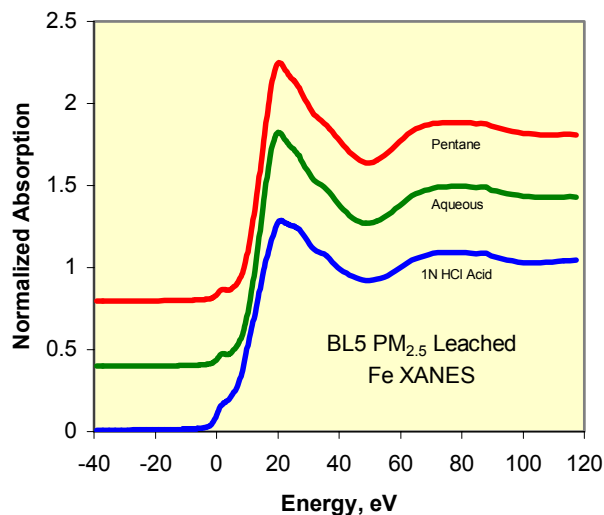


Figure 3. Iron XANES spectra of the BL5 $PM_{2.5}$ residue fractions after leachings in pentane, water and hydrochloric acid.

Similar analyses of the XAFS spectra of key elements in the leached coal PM samples are currently in progress. It is anticipated that similar insights and more complete speciation information about the metals in coal-derived PM will be obtained from such studies.

Conclusions

The combination of XAFS spectroscopy and a simple leaching protocol involving aqueous and acidic reagents provides significant speciation information about sulfur and key metals in PM derived from combustion of fossil fuels. Moreover, information is also obtained on readily soluble metal species that are of major interest to health effect studies of both source PM and also fine ambient PM.

Acknowledgements. The authors would like to acknowledge financial support from a NSF CRAEMS grant (CHE-0089133) and from a U.S. Department of Energy, FE/NPTO contract (DE-AC26-99BC15220). The XAFS experiments were conducted at the Stanford Synchrotron Radiation Laboratory, Stanford, CA, and the National Synchrotron Light Source, Brookhaven National Laboratory, NY, both of which are supported by the U.S. DOE.

References

- (1) Lighty, J. S.; Veranth, J. M.; Sarofim, A. F. *J. Air Waste Manage. Assoc.* **2000**, *50*, 1565-1618.
- (2) Huffman, G. P.; Huggins, F. E.; Shah, N.; Huggins, R.; Linak, W. P.; Miller, C. A.; Pugmire, R. J.; Meuzelaar, H. L. C.; Seehra, M. S.; Manivannan, A. *J. Air Waste Manage. Assoc.* **2000**, *50*, 1106-1114.
- (3) Shoji, T.; Huffman, G. P.; Huggins, F. E.; Linak, W. P.; Miller, C. A. *Energy Fuels* **2002**, *16*, 325-329.
- (4) Pattanaik, S.; Huggins, F. E.; Huffman, G. P.; Linak, W. P.; Miller, C. A. *ACS Fuel Chem. Div. Preprints* **2001**, *46(2)*, 626-627.
- (5) Linak, W. P.; Miller, C. A.; Wendt, J. O. L. *J. Air Waste Manage. Assoc.* **2000**, *50*, 1532-1544.
- (6) Miller, C. A.; Linak, W. P.; King, C.; Wendt, J. O. L. *Combust. Sci. Technol.*, **1998**, *134*, 477-502.
- (7) Koningsberger, D. C.; Prins, R. *X-ray Absorption*. Wiley & Sons, New York, 1988.

Fine Particles: Health Effects, Characterization, Mechanisms of Formation, and Modeling

Sarofim, A.F., Lighty, J. S., Eddings, E. G.

Department of Chemical and Fuels Engineering
University of Utah, Salt Lake City, UT 84112

Introduction

Dockery et al. (1993) published a study that showed that morbidity and mortality in six cities in the United States could be correlated with increased loadings of fine particles (defined as particles with aerodynamic diameters less than 2.5 microns). The data they provided now has been duplicated in many cities around the world (Pope, 1999, 2000). Pope (1999) studied the hospitalization of children in the Utah Valley during six-month intervals in three consecutive years during which a local steel mill was operating normally, was on strike, and was again operating normally. The data indicated that during the periods of September 1985 to February 1986, and September 1987 and February 1988 during which the steel mill was operating the mean and peak levels of PM₁₀ were considerably higher than during the intervening period from September 1986 to February 1987 during which the steel mill was closed by the strike. The hospitalizations of children during those three periods for bronchitis and asthma and for pneumonia and pleurisy showed a trend similar to the PM₁₀ concentrations. Additional studies show that the effects of high fine particle concentrations are not restricted to respiratory ailments, with significant evidence of cardiovascular effects (Pope, 2000). Recent studies (Peters, 2001) have shown acute effects with an increased risk of myocardial infarction from exposure to elevated concentrations of fine particles in the preceding two-hour period.

Although causality has been established between health effects and particle concentration, a mechanism has not. A number of hypotheses have been offered. These include some related to particle size, e.g., the postulate that the ultra-fine particles (< 0.01 microns) penetrate the interstitial regions of the lung and are deposited at a high enough frequency to overcome the natural cleansing abilities of the lung. Some are related to chemical composition, e.g., it has been postulated that the transition metals catalyze the formation of free radicals in the lung. Other chemicals implicated are acids, and a number of organic compounds. There are probably several agents that are responsible and it will take time to quantify their effects. Combustion sources are implicated because they are the dominant contributors to the fine particles that penetrate deeply into the lung, have a high surface to volume ratio that is important for the bioavailability of surface adsorbed species, and exist in high number concentration.

The following sections will review the particulate characterization for both ambient and source particles, mechanisms of fine particle formation, and models for calculating emissions.

Particle Characterization

Complete characterization of particles involves an enormous effort because of their physical and chemical complexity. Physical characteristics of importance are particle size, morphology, and crystallinity. Chemical characteristics include elemental composition, chemical form, chemical stratification, and isotopic ratios. The need for the information is partially dictated by the health impacts that are influenced by crystallinity (e.g., asbestos), elemental composition (e.g., lead, cadmium), valence state (e.g.,

arsenic, chromium), chemical state (e.g., mercury), and surface enrichment (e.g., sulfuric acid, trace toxic elements). Part of the information is needed for purposes of tracing the deposition patterns in the lung of particles (size and morphology) and part for source attribution (isotopic ratio, morphology, chemical signatures). In addition, knowledge of the temporal variations in concentration and composition are apparently important for determining the effects of particle elevation on cardiovascular disease.

The traditional method of characterizing particles has been by collection on filters, using cascade impactors to obtain size distribution, followed by detailed inorganic and organic analyses on the filters. Filter analyses provide the average composition of the particles in the deposit but there is increasing recognition of the need to know individual particle compositions. The review will present briefly recent developments on aerosol spectrometers that can provide the size and composition of single particles, knowledge of which can be important.

Ambient particles. Ambient particles are classified into a nucleation mode (<0.1 μm), accumulation mode (0.1 – 1.0 μm), and coarse mode (>1.0 μm). The composition of the fine particle mode (< 2.5 μm) is typically subdivided into crustal material, sulfate, nitrates, organic matter, and elemental carbon). The relative amounts will vary with location and time. There are certain discernable trends. Sulfates tend to be higher on the East Coast because of the impact of coal-fired power plants, nitrates are high in California with its high concentration of mobile sources, and crustal matter is high in arid areas. The relative importance of different sources can be determined using emission inventories or source attribution.

Estimates of the major sources of total particulate emissions (EPA, 1998) and the size distribution between the different size fractions for the different sources (Watson, 1999) show that, although fugitive or windblown dust are the major contributors to the total particulate emission, combustion sources are the dominant contributors to the emissions of fine particles. The combustion sources of interest are the internal combustion engine, particularly the compression ignition engine, stationary combustion sources, domestic heating, industrial applications, and power generation. There has been a continuous decrease in total particulate emissions in the U.S since the promulgation of the Clean Air Act in 1970. However, as the major sources are subjected to increasing control there is an increasing contribution from smaller sources. For example, the EPA estimates of particulate emissions from coal-fired power show a decrease in emissions from 1,700,000 tons in 1970 to 200,000 tons/year in 1998 (EPA, 1998). During this period the emissions from wood-fired stoves started at 400,000 tons/year in 1970 and after growing to a peak of slightly under a million tons in 1985 is back to a level of 400,000 tons/year. Wood stoves in 1998 were therefore estimated to emit twice as much particulate matter as coal-fired power plants. This is consistent with a trend towards having the small, less regulated sources, becoming the dominant contributors to the particulate emissions. Wood stoves, leaf burning, off road vehicles, snowmobiles, burning trash in barrels contribute to total particulate emissions a far greater fraction than is represented by the fraction of the total energy that they release because their emissions are uncontrolled. Fine particles in the atmosphere originate with both direct emissions and their generation by secondary reactions of sulfur dioxides, nitrogen oxides, and volatile organic hydrocarbons in the atmosphere, so that combustion sources contribute to ambient particulate loading both by their emission of both primary particles and sulfur and nitrogen oxides.

Stationary Sources. Well-operated stationary combustors will emit little unburned carbon so that their particulate emission is dominated by the inorganic elements. The elements will partition between a bottom ash, fly ash, and vapor. The size distribution of fly ash is approximately bimodal, with a submicron particles formed by the vaporization and condensation of mineral constituents and the residual having a particle size that will scale with the fuel particle size. The amount of submicron ash depends upon the fuel composition. It is of the order of one percent of the total mineral content for pulverized coal combustion but can be as high as 75 percent for black liquor recovery boilers. Many of the field studies of coal-fired power plants were aimed at obtaining the information needed for regulatory purposes so the measurements have focused on the total mass of the emissions. Selected field studies have determined the fractions of the trace elements entering a boiler that enter the flue gases and pass out of the unit through the stack. Additional efforts have focused on the effectiveness of air pollution control devices (APCD) in removing these potentially toxic substances. such studies provide the following information:

- The inorganic ash size distribution is multimodal. The submicrometer particles consist of aggregates of primary particles which have grown to 10–50 nm. The larger particles consist of spherical particles including cenospheres and plerospheres.
- Particles entering the APCD are essentially bimodal in terms of mass, with the order of one percent of the ash consisting of submicrometer particles and the larger residual ash falling into the 1 to 20 μm range.
- Particles in the 0.1 to 0.3 micrometer range have the highest penetration through the APCD compared to both larger and smaller particles; as a consequence the 0.1 - 1 μm particles form a larger fraction of the mass distribution leaving the APCD than they do in the uncontrolled combustion emissions .
- The submicrometer ash is enriched in volatile elements relative to the larger particles. The concentration of the trace elements within the submicrometer and supra micrometer ash fraction increases with decreasing particle size.
- The surfaces of the ash particles are also enriched in volatile elements relative to their core.
- The major influence on the fraction of ash that is vaporized is the temperature.

Mobile Sources. Mobile sources dominate the emissions of organic particles. The size distribution is again bi-modal with a nucleation mode (<10 nm) and an accumulation mode (10 – 300nm). The nucleation mode is often an artifact of the sampling since any nuclei formed in the engine will coagulate with the accumulation mode in the exhaust manifold. The particulate emission and size will be a strong function of load. Results of studies carried out on a number of on-road and off-road vehicles as well as military aircraft will be presented.

Submicron Particle Formation

The submicron particles are the ones that appear to be of greatest concern from a health standpoint, because of their high number density, ability to penetrate deep into the lung, and enrichment in toxic trace compounds. The mechanism of their formation is relatively well understood and models for calculating the amount and size of the submicron particle formation are now available. Descriptions of the progress that has been made in predicting the formation of inorganic and organic particles follow:

Submicron Ash Formation. A generalized formulation for the aerosol formation has been presented by Lockwood and coworkers (Abbas et al., 1996; Yousif et al., 1998). They set up the

aerosol dynamics equations, allowing for the nucleation and condensation of vapor species and for the coagulation of the aerosols. Here, we present a short description of the governing processes. As the vapors are cooled they can either nucleate or condense on the surface of existing aerosols. Analysis of this problem for the silica generated under conditions of interest to pulverized boilers shows that the silica will nucleate in the boundary layer of a particle for cooling rates above 200 K/s. For slower cooling rates the silica will condense on the surface of the existing residual ash particles.

The particle size distribution of the submicron ash can be calculated from the amount vaporized using the aerosol dynamic equations and the fact that the size distribution can be well approximated for the plug flow conditions of the laboratory reactors by Friedlander's self-preserving distribution (In this expression, particle size is given by $d = (5/6)^{-1/3}(k_c f_v t)^{2/5}$ where d is the volume average particle diameter, f_v is the fraction of the local volume occupied by particles, t is time, and k_c is the coagulation constant calculable from basic physical constants and the sticking coefficient) (Taylor and Flagan, 1982; Neville et al., 1982) consistent with results obtained in field studies (e.g., McElroy et al., 1981; Kauppinen and Pakkanen, 1990).

The trace element distribution of the submicron and residual particles can be determined by models that assume the vapors either condense on or react with the submicron particles or residual fly ash (Haynes et al., 1982; Linak and Wendt, 1993, 1994). Although the submicron ash particles contribute only of the order of one percent of the mass of the ash particles in the post combustion zone, their small size results in their providing the major fraction of the total surface area. These are also the particles that preferentially escape collection.

Soot Formation. Soot, unlike the inorganic oxide particles and condensable organic PM, is produced by a sequence of chemical reactions, some of which are essentially irreversible. The chemical reactions result in clusters of increasing molecular weight that grow into the measurable size range where the structures are considered particles. The smallest soot particles that have been observed by electron microscopy are in the range of 1 to 2 nm. A soot particle with a diameter of 1.5 nm and a specific gravity of around 1.8 contains about 160 carbon atoms. For soot, particle inception is defined as the particles first capable of measurement, in contrast to the nucleation process where there is a critical particle size at which nucleation occurs for a particular supersaturation. Despite the large literature on soot, the models of soot formation are still evolving. The three chemical kinetic components of a soot model are particle inception, surface growth, and surface oxidation. Coupled to the chemistry controlling the conversion of molecular precursors into solid soot are the physical models of particle coagulation and coalescence that determine the soot structure.

Soot forms under fuel-rich conditions where hydrocarbon fragments have a greater chance of colliding with other hydrocarbon fragments and growing rather than being oxidized to CO, H₂, CO₂, and H₂O. At equilibrium, soot exists when the C/O exceeds 1.0. Soot, however, is observed in flames of premixed hydrocarbons in air at C/O values of between 0.5 and 0.9. In diffusion flames soot forms even in the presence of excess air, since oxygen deficient conditions will always be found on the fuel side of the flame front .

One of the critical steps in soot formation is the formation of the first aromatic ring, usually benzene. It is for this reason that fuels having a high aromatic hydrocarbon content form soot easily. This has been described in terms of a threshold sooting index for various classes of organic compounds. Molecular weight growth

then proceeds with the formation of polycyclic aromatic hydrocarbons (PAH) that are considered to be precursors to soot. The formation mechanisms proceed through either a sequence of hydrogen abstractions and acetylene addition (HACA) and by the polymerization of the aromatic moieties that are produced. Applications of the HACA and parallel polymerization mechanism will be presented.

CFD Simulations

Over the last decade, CFD tools have been developed that are capable of effectively simulating the complex, reacting, multi-phase flows that exist in commercial boilers. These tools continue to evolve as more efficient and accurate descriptions of phenomena of interest are acquired. These CFD tools can be used to predict the effects of combustion process modifications on the vaporization of ash constituents. *GLACIER* is a CFD code developed to model turbulent flow, heat transfer, and chemical reaction. Its capabilities have been documented elsewhere (Adams and Smith, 1995; Davis et al., 1999). *GLACIER* provides Lagrangian information that is specific to statistical descriptions of clouds of particles based upon initial size and location. For example, a single burner in a boiler is often represented with ten to twenty particle cloud starting locations in an annular primary region and with eight to ten discrete particle sizes that are each representative of a single size range. (These bins are used to approximate the coal grind.) The results of the Lagrangian calculations can be used to generate mean values for a range of properties (gas temperature, oxygen concentration, particle temperature, particle size) that can be used in a post-process calculation to determine the vaporization of the important refractory ash species. The detailed tracking of particles as a function of starting location and initial particle size allow an in-depth evaluation of the either the formation and burnout of soot or the vaporization of ash from specific burners and particle size fractions. Illustrative applications will be provided to demonstrate the ability of such models to predict the size and composition of the submicron ash.

CONCLUDING REMARKS

The evidence for the association of increased respiratory and cardiovascular problems and increased particle concentrations is compelling and implicates combustion sources that dominate the ambient loading of submicron particles in the atmosphere. The mechanism for the health impact of these particles is uncertain but it is probable that there are multiple causes including the ability of ultrafine particles to penetrate the lung's epithelial layers and transition metals to catalyze free radical formation. It is therefore important to be able to characterize the size and composition of the particles emitted by combustion sources. There are multiple combustion sources that contribute to the emissions of the fine particles. In the presentation, the progress made in the understanding of the processes governing the particle size and chemical composition of submicron particles and their emissions will be reviewed. Although there are still many gaps in our understanding the progress is sufficient that the judicious use of the models in CFD codes can be used to predict the size and composition distribution of individual submicron particles. These theoretical developments are paralleled by experimental developments that permit the measurement of the size and composition of individual particles.

Acknowledgement. The authors have drawn extensively on previously publications, particularly Lighty et al, 2000 and Lee et al., 2000 in preparing this review. The work was supported in part by the SERDP and the Department of Energy.

REFERENCES.

- Abbas, T., Costen, P., De Soete, G., Glaser, K., Hassan, S., and Lockwood, F. C. (1996). *Proc. Combust. Inst.* Vol. 26, pp. 2487-2493.
- Adams, B.R., and Smith P. J. (1995). *P.J. Combust. Sci. Tech.* Vol. 88. p. 121.
- Chudnovsky, B. et al. (2001), "Reduction of NOx and Particulate Emissions from Coal-Fired Boilers by Modification of Coal Nozzles and Combustion Tuning", Paper presented at POWERGEN 2001.
- Barta, L.E.; Toqan, M.A.; Beér, J.M.; Sarofim, A.F. (1992). *Twenty-Fourth Symposium (International) on Combustion*, Pittsburgh, PA: The Combustion Institute, pp. 1135-1144.
- Charon, O.; Sarofim, A.F.; Beer, J.M. (1990). Distribution of mineral matter in pulverized coal, *Prog. Energy Combust. Sci.*, Vol. 16, pp.319-326.
- Davis, K.A., Valentine, J.R., Eddings, E.G. and Heap, M.P. (1999). The Mega Symposium: EPRI-DOE-EPA Combined Utility Air Pollutant Control Symposium, Atlanta, GA, p.13-31.
- Dockery, D.W. et al. (1993) *New England Journal of Medicine*, Vol. 329(24), pp. 1753-1759.
- Edwards, J. R., Srivastava, R. K., and Kilgroe, J. D. (2001). *JAWMA*, Vol.51, pp. 869-877.
- Elliott, J.F., Gleiser, M., and Ramakrishna, V. (1963). *Thermochemistry for Steelmaking*, Vol. 11, Addison-Wesley, Reading, MA.
- Ensr, D.S. et al. (1983). "Evaluation Electric Power Research Institute, report number EPRI CS-3252, Project 780-1,1983.
- EPA (1998) National air quality and emissions trends report, 1997, U.S. Environmental
- Flagan, R. C., and Taylor, D. D. (1982). *Proc. Combust. Inst.* Vol. 19, pp. 1227-1237.
- Haynes, B. S., Neville, M., Quann, R. J., and Sarofim, A. F. (1982) *J. Colloid Interface Sci.*, 87: 266-278.
- Haynes, B. S. (2001). "Vaporization of Minerals during Pulverized Coal Combustion", Seventh International Congress on Combustion By-Products: Origins, Fate, and Health Effects, June 4-6, 2001, National Institute of Environmental Health Sciences, Research Triangle Park, North Carolina.
- Helble, J.J. (2000). *Fuel Process. Technol.*, Vol 63, pp. 125-147.
- Huggins, F.E.; Huffman, G.P.; Lee, R.J. (1982). "Scanning electron microscope-based automated image analysis (SEM-AIA) and Mossbauer Spectroscopy: quantitative characterization of coal minerals," in *Coal and Coal Products: Analytical Characterization Techniques*, E.L. Fuller, Ed. American Chemical Society: pp. 239-258.
- Kang, S.-G.; Helble, J.J.; Sarofim, A.F.; Beér, J.M. (1988). *Twenty-Second Symposium (International) on Combustion*, Pittsburgh, PA: The Combustion Institute, pp. 231-238.
- Lee, C. M., et al. (2000). *Proc. Combust. Inst.*, Vol. 28, pp. 2375-2382.
- Lighty, J. S., Veranth, J. M., and Sarofim, A. F. (2000). *J. Air Waste Manage. Assoc.* Vol. 50, pp. 1565-1618.
- Linak, W. P., and Wendt, J. O. L. (1994). *Fuel Processing Technol.*, Vol. 39, pp. 173-198
- Linak, W. P., and Wendt, J. O. L. (1993). *Prog. Energy Combust. Sci.*, Vol. 19, p. 145.
- McCarthy, G.J.; Solem, J.K.; Manz, O.; Hassett, D.J. (1990). , *Minerals Research Society Symposium Proceedings*, Vol. 178, pp. 2-31.
- McElroy, M.W. et al. (1981). *Science*, Vol. 215, pp. 13-19.
- McNallan, M.J.; Yurek, G.J.; Elliott, J.F. (1981). *Combust.Flame*, Vol. 42, 45-60.
- Mohr, M., et al. (1996). *Aerosol Sci. Tech.*, Vol. 24, pp. 191-204.
- Neville, M., Quann, R. J., Haynes, B. S., and Sarofim, A. F. (1981). *Proc. Combust. Inst.* Vol. 18, pp. 1267-1274.
- Protection Agency, Office of Air Quality Planning and Standards, EPA 454 / R-98-016.
- Fisher, G. L., Chang, D. P. Y., and Brummer, M. (1976). *Science*. Vol. 192, p. 553.
- Flagan, R.C.; Friedlander, S.K. (1976). "Particle Formation in Pulverized Coal Combustion - A Review," in *Recent Developments in Aerosol Science*, Presented at the Symposium on Aerosol Science and Technology, Atlantic City, NJ, August 1976, D.T. Shaw, Ed. Wiley: New York, pp. 25-59.
- Niksa, S., Helble, J. J., Fujiwara, (2001). "Kinetic Modeling of Homogeneous Mercury Oxidation: the importance of NO and H₂O in predicting oxidation in coal-derived systems", Submitted to *Environmental Science and Technology*.
- Pope, C.A. (1999). *J. Environ. Med.*, Vol. 1, pp. 297-305.

Pope, C. A. (2000). *J. Environmental Health Perspectives*, Vol. 108, pp. 713-720.

Procaccini, C., et al. (1982). *Environmental Science and Technology*, Vol. 34, pp. 4565-4570.

Quann, R. J., and Sarofim, A. F. (1982) *Pro.c. Combust. Inst.* Vol. 19, pp. 1429-1440.

Raask, E. (1985). Mineral Impurities in Coal Combustion, Hemisphere Publishing Company, Washington.

Sarofim, A.F.; Howard, J.B.; Padia, A. S. (1977). *Combust. Sci. Technol.* Vol. 16, pp. 187-204.

Senior, C. L. et al. (2000). *Fuel Processing Technology*, Vol. 63, pp. 423-438.

Sloss, L.L.; Smith, I.M.; Adams, D.M.B.(1996). Pulverized coal ash — requirements for utilization, IEA Coal Research, IEACR/88

Steadman, E.N. et al. (1991).., "Coal and ash characterization: digital image analysis application," in *Engineering Foundation Conference on Inorganic Transformations and Ash Depositon During Combustions*, ASME, pp. 147-164.

Taylor, D. D., and Flagan, R. C. (1982). *Aerosol Sci. Technol*, Vol. 1, pp.103-117.

Ulrich, G.D.(1971).*Combust. Sci. Technol.*, Vol. 4, pp.47-57.

Watson, J.G.; Chow, J.C., (1999). Reconciling Urban Fugitive Dust Emissions Inventory and Ambient Source Concentration Estimates: Summary of Current Knowledge and Needed Research, Desert Research Institute, DRI Document No. 6110.4D2.

Wigley, F.; Williamson, J.; Gibb (1997).W.H. The distribution of mineral matter in pulverized coal particles in relation to burnout behaviour, *Fuel* Vol. 76, pp.1283-1288.

Wilemski, G.; Srinivasachar, S.; Sarofim, A.F.(1991). "Modeling of mineral matter redistribution and ash formation in pulverized coal combustion," in *Engineering Foundation Conference on Inorganic Ash Transformations and Ash Deposition During Combustion*, ASME, pp. 545-564.

Wu, H.; Bryant, G.; Benfell, K.; Wall, T.(2000). *Energy Fuels*, 2000, Vol. 14(2), pp. 282-290.

Ylatalo, S.I., and Hautanen, J. (1988). *Aerosol Sci. Tech.*, 29,17-30.

Yousif, S., Lockwood, F. C., and Abbas, T. (1998) *Proc. Combust. Inst.*, Vol. 27, pp. 1647-16

INVESTIGATION OF FINE PARTICULATE MATTER FROM A DIESEL ENGINE USING SCANNING TRANSMISSION X-RAY MICROSPECTROSCOPY

Artur Braun, Naresh Shah, Frank E. Huggins, Gerald P. Huffman

CFFS/CME, University of Kentucky
Lexington, KY 40506

Kerry Kelly and Adel Sarofim

Chemical and Fuels Engineering, University of Utah
Salt Lake City, UT 84112

Sue Wirick and Chris Jacobsen

Department of Physics and Astronomy, State University of
New York, Stony Brook, NY 11794

Introduction

Recently, the Environmental Protection Agency (EPA) has imposed new regulations concerning airborne particulate matter from commercial combustion sources, with a particle size smaller than 2.5 micrometer. This includes, for instance, soot as it originates from diesel engines. Soot can be characterized in various ways [1]. Most important, its chemical composition has to be known. Therefore, various spectroscopic techniques are employed to gather information on which elements or compounds to which amount are present in the particles. Also, the structure of the soot and the size of its particles may have an impact on its environmental activity, starting with its size. Soot consists predominantly of carbon, which may be porous and may contain trace elements and other parasitic compounds such as residual fuel and lubricants.

The structure of soot from engines depends strongly on operation parameters like *idle* or *load speed* and *fuel* and *lubricant composition*. X-ray Diffraction (XRD) and Nuclear Magnetic Resonance Spectroscopy (NMR), for instance, are common tools to study the porosity or the microstructure of soot particles, yet they only provide a statistical average of those properties for many particles. To assign particular phases to particular regions on the sample, probes with a local spatial resolution are required. Scanning transmission X-ray microspectroscopy (STXM) is such a technique [2,3]. It is based on synchrotron radiation and allows simultaneous X-ray imaging and molecular speciation of thin samples. It has been applied extensively to carbonaceous materials and is a promising technique for investigating the molecular structure and microstructure of fine diesel particulate matter (DPM).

Near the carbon K-shell absorption edge, the transmitted X-ray intensity undergoes significant variation with energy, and by digital image processing and subtraction algorithms, chemical inhomogeneities can be identified with a spatial resolution of approximately 50 nm.

We present the first results of an investigation of the molecular structure of carbon in DPM by STXM. The DPM samples were produced in a small diesel engine test facility at the University of Utah equipped with extensive online monitoring apparatus. It is demonstrated that one can discriminate and localize aromatic and aliphatic groups in single DPM particles and distinguish unburned fuel and oil from solid soot.

Experimental

Conventional diesel was combusted in a test engine, and the soot particles were collected on a filter following the exhaust. Part

of the soot was removed from the filter, immersed in acetone and then one drop of this solution was placed on a Si_3N_4 window for further analysis in the STXM. STXM experiments were carried out on beamline X1A at the National Synchrotron Light Source in Brookhaven National Laboratory [3]. Scans with a lateral resolution of 50 nanometers were taken at X-ray energies that ranged from 280 eV to 293 eV, in steps of 0.05 eV. Thus, a stack of 280 images, each at a different X-ray energy, is obtained. The data analysis program, based on IDL programming language, provides graphic tools to single out regions of particular interest.

Results and Discussion

Figure 1 displays X-ray diffractograms of soot generated in a diesel engine at idle and at load condition. At a diffraction angle of about 26° , there is a prominent diffraction peak arising from the distance of stacked aromatic rings, as they appear in graphite. At about 20° , a shoulder or peak arising from the width of aliphatic side chains is visible. Comparison of both diffractograms reveals that, under load condition, the graphitization is more pronounced than under idle speed, at the cost of the abundance of aliphatic side chains. Thus, using additives, it is possible to suppress graphitization of soot at least under idle condition.

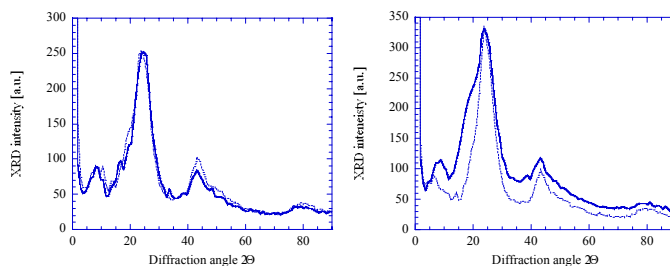


Figure 1: Left - X-ray diffractograms of soot particles from a diesel combustion engine at load (dotted line) and idle (solid line) speed. Right - soot from same diesel that contained additives.

On the next page, Figure 2 displays a STXM micrograph (left picture) of an area of approximately $10 \mu\text{m} \times 10 \mu\text{m}$, obtained at an X-ray energy of 284.6 eV. Micrographs were scanned at energies between 280 and 293 eV, in steps of 0.1 eV. The micrograph includes an inset of a magnified region with one single particle that we have studied.

To the right, in Figure 2, a series of carbon K-edge absorption spectra is shown. They were obtained from the single particle shown in the inset. The carbon K-shell absorption edge is located at about 283 eV. At about 285 eV, we find the $\pi_{1,2}$ transition, while the somewhat less pronounced peaks at 288 eV are termed $\pi_{3,4}$. The π^* resonance at 285 eV is indicative to a transition from a 1s state to a 1p state and is observed for molecules with carbon double bonds and triple bonds. The spectra allow for the discrimination between carbon in aromatic and aliphatic bonding conditions. Using conventional X-ray near edge absorption spectroscopy (XANES), or XRD, one can make a only global distinction between the aromatic and aliphatic partitions in the carbon sample. With the use of STXM, however, we are able to trace back locations with more graphitic or more amorphous carbon.

The STXM data analysis software allows one to select specific single regions in the micrograph and to obtain the corresponding XANES spectra. We have selected one such particle as shown in Figure 2. The particle was encircled, and the transmitted intensity of the circle line was defined as the background signal I_0 . The inset shows how the particle was encircled (highlighted pixels which build

the circle) and how the center of the particle was selected (highlighted pixel in center). From the ratio of both intensities, the X-ray optical density (μd) of the particle center was determined: $I_p = I_0 \cdot \exp(-\mu d)$. This procedure yields the XANES spectrum of one particle region, and a whole set of such spectra from different regions of one particle are shown on the right side of Figure 2.

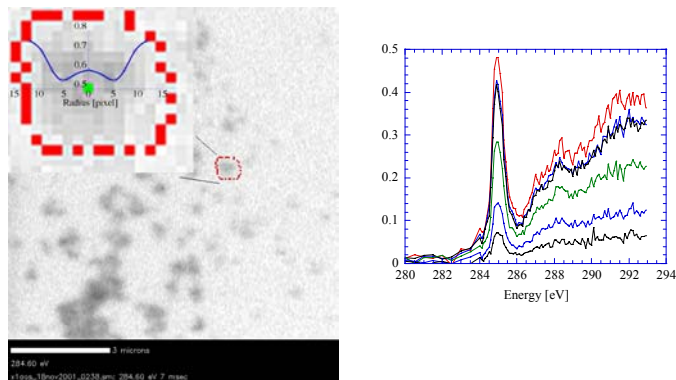


Figure 2: Left - STXM micrograph with particles dispersed on Si₃N window. Inset with magnified single particle and imprinted differential concentration profile. Right - series of carbon K-edge XANES from different regions on one particle

In the next step, the pixel in the center of the particle was encircled by the smallest possible pixel circle, while the center pixel itself was omitted. The summarized intensity of this circle was taken I_p , while I_0 was not changed. This procedure yields the second XANES in a series of seven XANES, and finally allows us to build a line profile scan across the entire particle. In the next stage of analysis, the heights of the $\pi_{1,2}$ and $\pi_{3,4}$ transitions were determined and their ratio was formed. This ratio is plotted versus the radius of the circles of data gathering in the inset in figure 2. The curvature of the ratio versus the distance from the sample center shows that the particle center is made of carbon with predominantly $\pi_{1,2}$ transitions. The boundary probably contains more aliphatic carbon (residual fuel, lubricant), which was washed out from the particle when the sample was prepared with acetone.

In Figure 3, we see a micrograph of a different sample region, taken at an X-ray energy of 285.11 eV. The images show inhomogeneities (bright, on dark background), which can be assigned with soot particles of a size smaller than one micrometer. The background intensity I_0 is recorded in the upper right corner (marked dark), and the transmitted intensity I_p is marked bright. In the left micrograph, the region of interest is the wash-out corona around some particles, this is, a region around the sample where washed out residual fuel and oil are located.

As an inset in the image, the optical density (the logarithm of the bright region intensity I_p divided by the dark region intensity I_0) is shown versus the X-ray energy. The micrograph on the right displays the same X-ray image, but now only the cores (bright dots) of particles are selected for analysis. The corresponding XANES spectrum shows peaks at exactly the same positions as the wash out corona does. However, peak intensity ratios are quite different. The washed out region has a pronounced $\pi_{3,4}$ transition peak, while the particle centers have a pronounced $\pi_{1,2}$ transition peak.

The carbonaceous soot particles are very likely porous aggregates and loaded with residual fuel and lubricant. Immersed in acetone and then poured on a sample slide, a corona can be found around the particles.

Outlook

We have demonstrated that we can single out particular particles and particle regions of interest with STXM and analyze them for the type of carbon present. Due to the chemical contrast, we are able to distinguish between aromatic and aliphatic types of carbons and can assign them to particular sample regions. Our next step will be to collect a set of reference spectra from materials, which are important for diesel combustion; those include commercially available diesel, lubricants, additives, as well as model substances such as octane and hexadecane. This hopefully will enable us to get a more detailed picture about the spatial distribution of species in DPM.

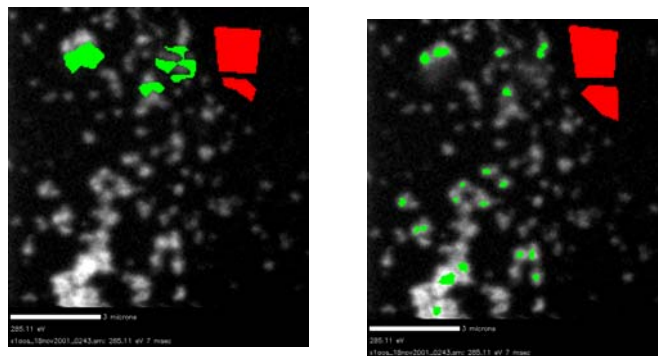


Figure 3: Left - X-ray micrograph with highlighted sample regions for washed out material (bright), background signal (dark), and corresponding XANES. Right - only the particle centers are highlighted, with corresponding XANES.

Acknowledgment

This research has received financial support by the National Science Foundation, grant # CHE-0089133. NSLS is operated by SUNY for the United States Dept. of Energy, Contract # DE-AC02-76CH-00016.

References

- (1) Huffman, G.P.; Huggins, F.E.; Shah, N.; Pattanaik, S.; Meuzelaar, H.L.C.; Jeon, Sun Joo; Smith, D.; Seehra, M.S.; and Manivannan, A. Prepr. Pap. - *Am. Chem. Soc., Div. Fuel Chem.*, **2000**, 45 (3), 441-445.
- (2) Thieme, J.; et al.; eds.; *X-ray Microscopy and Spectromicroscopy* (Springer, Berlin **1998**).
- (3) Jacobsen, C; Kirz, J., *Nature Structural Biology* **1998**, 5, 650-653.

Low temperature destruction of chlorinated hydrocarbons over lanthanide oxide-based catalysts

Pieter Van der Avert¹; Robert A. Schoonheydt¹; Bert M. Weckhuysen²

¹ Center for Surface Chemistry and Catalysis, KULeuven, Kasteelpark Arenberg 23, 3001 Heverlee, Belgium.

² Department Inorganic Chemistry and Catalysis, Debye Institute, University Utrecht, Sorbonnelaan 16, 3508 TC Utrecht, Netherlands.

Introduction

Chlorinated hydrocarbons (CHC's) are frequently applied in dry cleaning processes, in degreasing operations and as organic solvents because of their inertness and ability to dissolve organic solvents. The crucial method to remove those noxious products from flue gases is thermal incineration. During thermal incineration, the products are burned at temperatures higher than 1300°C to avoid the formation of dioxins and polychlorobiphenyls (PCB's). A first alternative is the catalytic oxidation of CHC's at temperatures between 300°C and 550°C over supported noble metal catalysts⁽¹⁾ (e.g. Pt, Pd and Au) and supported transition metal oxide catalysts⁽²⁾ (e.g. VO_x, MnO_x, FeO_x, CoO_x, NiO_x, CrO_x) to CO₂ and Cl₂. A second alternative for incineration is hydrodechlorination (HDC) in which a CHC is transformed in the presence of hydrogen into an alkane and HCl. Commonly used catalysts are supported Ni, Pd and Pt. We present a new catalytic system based on lanthanum oxides, which is able to destroy CHC's (including CCl₄) in the presence of steam.

Experimental

Preparation. The lanthanum oxide-based catalysts were prepared via the incipient wetness impregnation technique with aqueous solutions of the metal compounds in their acetate form (Aldrich, > 99.9%). Al₂O₃ (Condea) with a specific surface of 220 m²/g, was used as support. The catalysts were granulated and the fraction of 0.25-0.50 mm was used for further catalytic experiments.

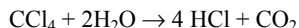
Experimental set up. Catalytic tests were performed in a fixed-bed reactor at atmospheric pressure. Before the reaction started, the catalyst was calcined overnight in an oxygen flow of 600 ml.h⁻¹ at 450°C. During the reaction, the feed consisted of a helium flow, which was lead through a saturator filled with CCl₄ (VEL, p.a.) and maintained at 0°C. All the tubes are in Viton, while the total He flow was set at 480 ml.h⁻¹. This resulted in a maximum CCl₄ loading of 48000 ppm (v/v). The space velocity (GHSV) was 800 h⁻¹. Water was added to the reactor at a rate of 1.2 ml.h⁻¹ and evaporated when in contact with the reactor walls and bed. The reactions were performed at 250°C, 300°C and 350°C. After the reactor, the condensate was trapped in an impinger at room temperature. The remaining gases were guided to a gas chromatograph (HP 4890D with FID detector and methanator) and analysed using a packed Hayesep Q CP column (80-100 mesh, 3 m length).

Results and discussion

When the activities (at 350°C, adding 0.02 ml H₂O min⁻¹) of the different oxides are compared, the activity towards the conversion of CCl₄ decreases in the order:



No other products than HCl and CO₂ are found in the effluent gas and condensate. Thus the overall reaction can be written as:



Further experiments and characterization were performed with La₂O₃/Al₂O₃ which activity increases with increasing La-loading.

Pure Al₂O₃ reveals a conversion of around 40%. With low loadings, the activity remains around this level. From 4 wt%, the activity proportionally increases with higher La-loading. At 10 wt%, the activity reaches 100% conversion and remains constant for higher La-loadings. This activity can be maintained for at least 48 hours.

Figure 1 shows the activity of the 10 wt% La₂O₃/Al₂O₃ catalyst for the destruction of CCl₄ at different temperatures, changing the amount of added water.

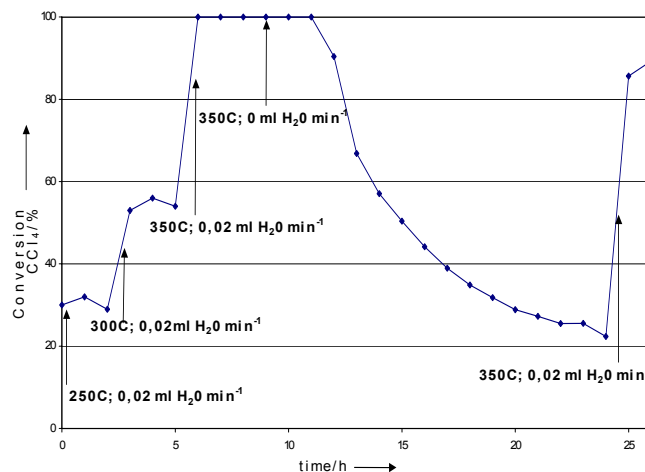


Figure 1. Influence of reaction temperature and the presence of steam on the conversion of CCl₄ over La₂O₃(10 wt%)/Al₂O₃.

As expected, there is an increase in activity with increasing temperature in the presence of H₂O. At 250°C, the catalyst shows a conversion of 30%. This rises to 53% at 300°C and eventually peaks at 100% at 350°C. After 3 hours, the water source is switched off. As can be seen from figure 1 the conversion becomes complete for three hours before the activity decreases systematically. After 15 hours, only 22% conversion is achieved. When steam is added again after 16 hours, the activity increases, till the former level and decreases again. From these experiments, we can conclude that water is a necessary agent for the in situ regeneration of the catalyst. The complete conversion just after switching off the water is probably due to the destructive adsorption of CCl₄ on the surface⁽³⁾.

Table 1 shows, besides our findings, an overview of some of the most important catalysts for the catalytic oxidation of CCl₄ at 350°C with increasing activities. As table 1 reveals the present catalyst is much more active than the so far published catalytic systems. The second column shows the destruction capacity in 10⁶ ppm/hour. The La₂O₃/Al₂O₃ catalyst can destroy 42.3x10⁶ ppm/hour at 350°C, while other catalysts achieve an activity at the same temperature of maximum 15x10⁶ ppm/hour. This means that the catalyst based on La₂O₃ is at least a three times more active for the catalytic destruction of CCl₄. Weiss et al. already reported about the catalytic hydrolysis of CCl₄ in the presence of an excess of steam to HCl and CO₂ over magnesium oxide⁽⁴⁾. But they observed a significantly lower activity than we do.

Table 1. Overview of the activities of different catalytic systems for the destruction of CCl₄ at 350°C.

Catalyst	Destruction capacity (10 ⁶ ppm/h)	Reference
LaCoO ₃	0.6	(5)
Co-Y	1.4	(7)
Cr-Y	1.4	(7)
LaMnO ₃	2.4	(6)
Cr ₂ O ₃ /Al ₂ O ₃	5.3	(8)
Pt,Pd or Rh/TiO ₂	15	(8)
La ₂ O ₃ /Al ₂ O ₃	42.3	This work

Conclusions

We have found that among the lanthanide oxides La₂O₃/Al₂O₃, Nd₂O₃/Al₂O₃ and Nb₂O₅/Al₂O₃ show the highest activity for the conversion of CCl₄ to HCl and CO₂ in the presence of steam and this for at least 48 hours. Conversions of 42.3 10⁶ ppm/hour at 350°C and selectivities of 100% were achieved. Steam is the necessary agent during the process. The activity increases with increasing La-loading and reaches its maximum at 10 weight percent La on Al₂O₃.

References

- (1) Bond, G.C.; Sadeghi, N. *Journal of Applied Chemistry and Biotechnology*, **1975**, *25*, 241-248.
- (2) Krishnamoorthy, S.; Rivas, J.A.; Amiridis, M.D. *Journal of Catalysis*, **2000**, *193*, 264-272.
- (3) Weckhuysen, B.M.; Rosynek, M.P.; Lunsford, J.H. *Physical Chemistry and Chemical Physics* **1999**, *1*, 3157-3162.
- (4) Weiss, U.; Rosynek, M.P.; Lunsford, J. *Chemical Communications* **2000**, *5*, 405-406.
- (5) Sinquin, G.; Hindemann, J.P.; Petit, C.; Kiennemann, A. *Catalysis Today*, **1999**, *54*, 107-118.
- (6) Sinquin, G.; Petit, C.; Libs, S.; Hindermann, J.P.; Kiennemann, *Applied Catalysis B: Environmental*, **2000**, *27*, 105-115.
- (7) Chatterjee, S.; Greene, H.L.; Joon Park, Y. *Journal of Catalysis*, **1992**, *138*, 179-194.
- (8) Lester, G.R. *Catalysis Today* **1999**, *53*, 407-418.

MERCURY SPECIATION AND CONCENTRATIONS AT ESP IN A 100MWE COAL-FIRED POWER PLANT

Rongcai Xie¹, Yufeng Duan¹, Yan Cao¹, Ling-Chuan Li¹, Shawn Kellie¹, Wei-ping Pan¹, John T. Riley¹, Ken Ho², Paul Chu³, and Arun Metha³

- (1) Combustion Laboratory, Department of Chemistry, Western Kentucky University, 1 Big Red Way, Bowling Green, KY 42101,
- (2) Illinois Clean Coal Institute
- (3) Electric Power Research Institute

Introduction

EPA has estimated that during the period 1994–1995 annual emissions of mercury from human activities in the United States were 159 tons. Approximately 87% of these emissions were from combustion sources. Coal-fired utilities in the U.S. were estimated to emit 51 tons of mercury per year into the air during this period¹. So, mercury pollution of the environment from coal combustion has resulted in worldwide contamination of large areas of soils and sediments and led to elevated atmospheric mercury level. Mercury and its compounds have been considered very potential neurotoxins. Once mercury has deposited on land or water, it can transform into methylmercury, an organic form, and thereby enter the food chain. Humans are most likely to be exposed to methylmercury through consumption of fish. They bind to the sulfhydryl groups of enzymes and proteins, thereby inactivating vital cell function.

A recent report by the Environmental Protect Agency (EPA) on emissions of hazardous air pollutants by electric utilities predicted that emissions of air toxics from coal-fired utilities would increase by 10% to 30% by the year 2010². To reduce the risk mercury poses to people's health, the Environmental Protection Agency (EPA) is announcing that it will regulate emissions of mercury and other air toxics from coal- and oil-fired electric utility steam generating units (power plants).

However, the current knowledge of mercury transformations in coal combustion flue gas is based largely on thermodynamic modeling and experimental investigations of mercury reactions in simulated flue gases, and, to a limit extent, on the interpretations of field test data.

To further these studies on mercury emissions and gas-phase transformations of mercury coal-fired power plant, Western Kentucky University (WKU) recently established a mobile mercury emissions monitoring lab (MMEML). The lab was constructed using a 53 ft. tractor-trailer that was divided into three separate rooms: storage, preparation room, and analysis room. The lab contains facilities to perform both continuous emissions monitoring mercury and the Ontario Hydro method of mercury analysis. Among the instrument available in the lab are a continuous emission monitor (CEM) with pretreatment and speciation module an atomic absorption spectrometer with automated sampler. The MMEML was recently moved to a 100MWth, wall-fired combustor with low-NOx burners. Electrostatic Precipitator (ESP) is one of the most widely used particulate collection devices. In order to fully explore the potential of this pollution control equipment, the mercury speciation and concentrations at the inlet and outlet of the ESP were measured. The mercury transformation mechanism through ESP will be discussed.

Experimental

Coal Samples. The coal used in this study is the bituminous coal. Chlorine concentration ranges from 200–500 ppm while mercury concentrations range from 80–120ppb.

Characterization Methods. Mercury speciation and concentrations at the inlet and outlet of the ESP were measured with PS Analytical Ltd. Sir Galahad mercury CEM, an automated continuous emission monitor for elemental mercury and total vapor-phase mercury in combustion flue gases. The CEM consists of mercury speciation module and the detector. The speciation module converts oxidized mercury in the sample gas to elemental mercury by means of a proprietary aqueous reagent, allowing separate detection of elemental mercury and total mercury. All parts of the test unit are Teflon, Teflon-lined, or glass, and the entire system, including the gas manifold for mixing the gases, is heat-taped to maintain a constant temperature. High span test will make sure the accuracy of the instrument. Sample ports are before ESP (port 2) and after ESP (port 3). Temperature at port 2 is about 153 °C, while temperature at port 3 is about 146°C.

Results and discussion

Chlorine-containing species have been shown to be the most important for oxidation of elemental mercury in flue gas. In this experiment, we also compare the mercury speciation and concentrations in the flue gases of two different coal-containing coals. The result is shown in **Figure 1**. It is found that the percentage of elemental mercury in the flue gas increases with a decrease the chlorine content. The result can be explained that elemental mercury will react with chlorine atom or HCl. More chlorine content, the lower elemental mercury concentration^{3,4}.

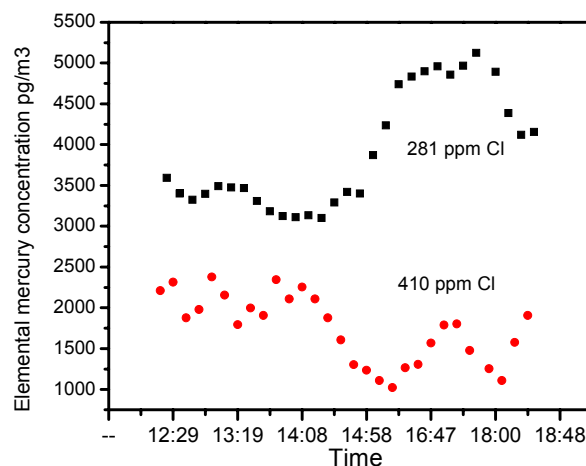
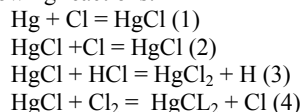


Figure 1: Effect of Cl content on the elemental mercury concentrations before ESP

Possible paths for mercury transformation may be due to following reactions:



Due to the high energy barrier of the $\text{Hg} + \text{HCl}$ reaction, the direct elementary oxidation of mercury by HCl will not occur under the present conditions. This suggests that the oxidation occurs via an intermediate derived from HCl or Cl_2 . One likely candidate is atomic

chlorine. The temperature dependence of the oxidation suggests a reactive intermediate whose concentration is promoted by high temperatures. This does not support Cl, whose concentration increases with lower temperatures. The fast oxidation of mercury at lower temperature via reaction (1) has been reported in the literature $k_2 = 1.95 \pm 1.05 \times 10^3 \text{ cm}^3/\text{mol s}^{5,6}$.

ESP control devices have been used to control PM emissions for over 80 years. These devices can be designed to achieve high PM collection efficiencies (greater than 99%), part of gaseous mercury absorbed on the surface of PM can be removed. In this work, we also measure the mercury speciation and concentrations before and after ESP to explore the effect of mercury removal by ESP. **Figure 2** and **Figure 3** are total mercury concentration and elemental mercury concentration before and after ESP, respectively. Both figures indicate mercury concentrations decrease after ESP. Total mercury concentration decreases about 15% though ESP, while elemental mercury concentration changes a little. These results conform that oxidized mercury may be absorbed on the surface of PM to become particulate mercury.

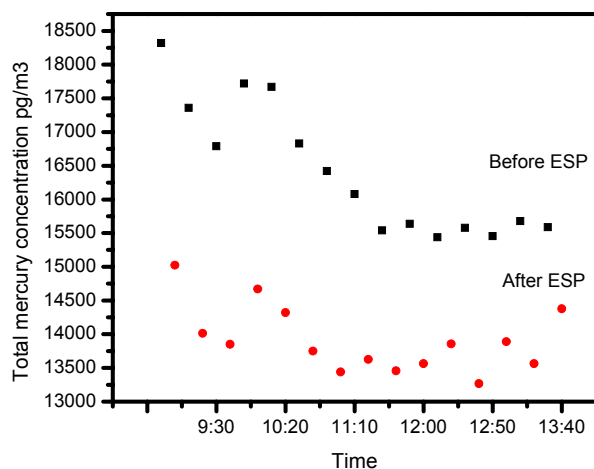


Figure 2. Total mercury concentrations before and after ESP

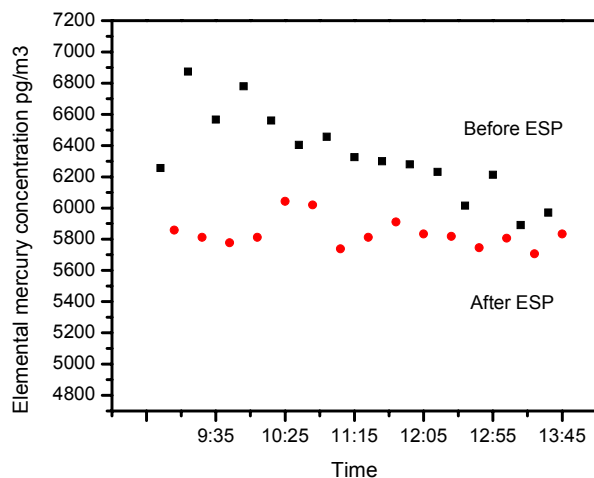


Figure 3. Elemental mercury concentrations before and after ESP

In addition to aiding in adsorption, laboratory and pilot-scale studies have shown that solids such as activated carbon and fly ash can act as catalysts for the oxidation of elemental mercury. A study of

fly ash from five different coals showed that the fly ash converted gaseous elemental mercury to a mixture of gaseous oxidized mercury and adsorbed mercury⁴.

Hg in coal can not be destroyed and will volatilize during combustion and subsequently condense to form metallic particles during the cooling of flue gas. These metallic particles are submicron in size, which may not always be effectively collected by conventional air pollution control system. Various existing emissions control technologies such as electrostatic precipitators (ESP), fabric filters, and fluid gas desulfurization (FGD) system have been evaluated for their ability to reduce mercury emissions from combustion sources. However, previous studies indicate that it is difficult and uneconomic to control the volatilization of metals during high-temperature processes. The mean removal efficiency of ESP and fabric filter was about 30%, while FGD can remove between 8% and 90% of mercury⁷. Percentage removals of mercury should depend on electrical voltage, temperature, retention time and other factors. However, it is not difficult to find that the percent mercury removal by ESP in this experiment is limited. A special method for mercury removal should be developed.

Acknowledgment. This work was supported by Electric Power Research Institute, and the Illinois Clean Coal Institute under contracts EPRI Project Number:EP-P6549/C336 and EP-P7403/C3763 as well as ICCI Project Number: 01-1/2.4A-1

References

1. Constance, L. S., Adel, F. S., Taofang Z., Joseph, J. H., Ruben, M. P., *Fuel Processing Technology*, **2000**, 63,197-213
2. Keating, M. H., et al, Mercury Study Report to Congress, Vol. I: Executive Summary, EPA-452/R-97-003
3. Kenlei, L., Ying, G., Shawn, K., Wei-Ping, P., John, T. R., Ken, K. H., Arun, K. Mehta, *Combust. Sci. and Tech.* **2001**, 164, 145-162
4. Kenlei, L., Ying, G., John, T. R., Wei-Ping, P., *Energy&Fuels*, **2001**, 15, 1173-1180
5. Rebecca, N. S., John, C. K., Nick, M. M., *Fuel Processing Technology*, **2000**, 65-66, 423-438
6. Horne, D. G., Gosavi, R., Strausz, O. P., *J. Chem. Phys.*,**1968**, 48, 4758-4764
7. Liu, W., Vidic, R. D., *Environ Sci Technol*, **1998**, 32, 531-538

NETL'S AMBIENT AIR FINE-PARTICULATE CHARACTERIZATION PROGRAM: FIRST YEAR RESULTS

Richard R. Anderson¹, Donald V. Martello¹, Curt M. White¹ and Delbert J. Eatough²

¹United States Department of Energy, National Energy Technology Laboratory, P.O. Box 10940, Pittsburgh, PA 15236-0940 USA

²Department of Chemistry and Biochemistry, Brigham Young University, E114 BNSN, Provo, UT 84602

Introduction

In July 1997, the U.S. Environmental Protection Agency revised the National Ambient Air Quality Standards (NAAQS) by setting limits on the concentration of ambient air particulate matter with an aerodynamic diameter of 2.5 micrometers or less, PM_{2.5}. As one component of a comprehensive program to assess the impact that this stringent regulation will have upon the future technology of fossil-fuel-fired electric power generation, the U.S. Department of Energy has established a state-of-the-art ambient-air fine-particulate monitoring station at the National Energy Technology Laboratory (NETL) -Pittsburgh. In particular, this research program is directed toward determining the method and degree by which fossil-fuel-fired electric power generating stations contribute to the particulate matter load in ambient air.

Sampling for the NETL PM_{2.5} research program was initiated at the Pittsburgh NETL sampling site, located in a suburban area 20 km southwest of the Pittsburgh city center, in October 1999. This manuscript gives a brief overview of the sampling program and an example of the results for the initial year of operation.

Experimental

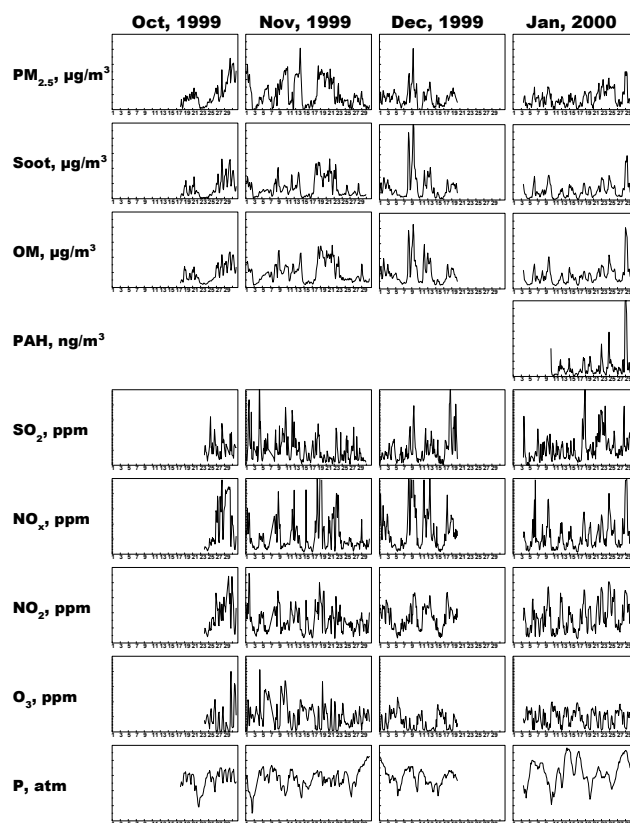
The air-monitoring site is located on an open hill at the NETL Pittsburgh facility. The specific location of the sampling station was chosen to take advantage of an existing meteorological tower that could supply full weather data for the program. The air monitoring station consists of a new 715 ft² indoor facility housing equipment to monitor gaseous pollutants (O₃, SO₂, CO, NO_x, NO and NO₂) and PM_{2.5} particulate carbon and polycyclic aromatic hydrocarbons (PAH) continuously. In addition, a fully instrumented, fourteen bay rack was constructed to support a variety of PM_{2.5} samplers.

Equipment installed at that time included; a PM_{2.5} Partisol-Plus Model 2025 FRM Sequential Air Sampler (R&P) for the 24-h determination of PM_{2.5} mass, a PM_{2.5} Model 1400AB TEOM Ambient Particulate Monitor (R&P) for the continuous measurement of PM_{2.5} mass, a PM_{2.5} Model 5400 Ambient Carbon Particulate Monitor (R&P) for the continuous measurement of PM_{2.5} carbon, a PM_{2.5} RASS 2.5-400 Speciation Sampler (Andersen) for the periodic determination of fine particulate composition, a PAS 2000 Real-time PAH Monitor (EcoChem Analytics Model PAS 2000) for the continuous measurement of particulate PAH concentration, and monitors for the continuous measurement of SO₂(g) (API Model 100A Chemiluminescent Monitor), O₃ (API Model 400A Photometric Monitor), CO (API Model 300), and NO_x and NO₂ (API Model 200A Fluorescent Monitor), and a highly instrumented meteorological tower (Climatronics). The various gas analyzers were calibrated weekly using a Dynamic Dilution Calibrator (API Model 700) and certified gas standards. The mass on all 24-h integrated filter samples collected with the various PM_{2.5} integrated samplers was determined at the nearby Mine Safety and Health Administration laboratory using the FRM PM_{2.5} protocols.⁽¹⁾

Results and Discussion

Presented in Table 1 is a reduced summary of the some of the data gather in the initial year of this study. The annual average concentration of PM_{2.5} for this period determined by a TEOM monitor was 11.8 µg/m³. Annual average concentrations of PM_{2.5} mass determined using a FRM sampler were higher, averaging 14.8 µg/m³. The greatest difference between the TEOM monitor and the PM_{2.5} FRM sampler were seen during winter and summer months. The differences are attributed to semi-volatile material measured by the PM_{2.5} FRM but not retained on the heated filter of the TEOM monitor.

The continuous measured concentrations of PM_{2.5} mass and carbonaceous material, and of gas phase NO_x, NO₂, SO₂, CO, and O₃ were averaged to a common three-hour basis for the period from October 1999 through September 2000 for use in trend analysis. The following figure is an example of this three-hour data from the first quarter of the study.



Periodic peaks in PM_{2.5} concentrations were seen throughout the year with the most frequent and highest concentration episodes occurring in the summer. Meteorological and back-trajectory analyses indicate that these peaks in PM_{2.5} are associated with the transport of pollutants from outside the NETL sampling site region. The most frequent episodes and the highest concentrations are associated with transport to the NETL site from the Ohio River Valley to the west and southwest.

Table 1. Monthly Average Concentrations of Monitored Species at the NETL Site During 18 October 1999 through 30 September 2000.

Species	Measure-ment	Oct	Nov	Dec	Jan	Feb	Mar	Apr	May	Jun	Jul	Aug	Sep	Annual Avg
PM _{2.5} Mass, µg/m ³	TEOM	11.2	10.9	8.0	7.9	9.8	8.7	8.8	15.7	16.3	14.5	15.7	11.0	11.5
PM _{2.5} Mass, µg/m ³	TEOM ^a	11.2	10.7	8.0	7.8	9.8	8.6	9.0	16.5	17.0	14.6	16.6	11.3	11.8
PM _{2.5} Mass, µg/m ³	FRM ^a	13.8	14.3	12.1	12.4	14.2	11.0	11.1	17.4	19.7	17.6	20.2	14.0	14.8
PM _{2.5} OM, ^b µg/m ³	R&P C	3.8	4.1	4.2	3.5	3.8	3.0	4.9	5.8	4.4	5.9	4.6	2.8	4.2
PM _{2.5} EC, ^c µg/m ³	R&P C	0.6	0.6	0.7	0.5	0.6	0.4	0.6	0.6	0.7	0.8	0.9	0.7	0.8
PM _{2.5} PAH, fA/m ³	EcoChem				4.7	4.9	4.1	3.5	2.6	2.8	3.4	4.1	5.0	3.9
SO ₂ , ppb	API	11.1	10.6	10.5	12.2	10.1	9.2	8.2	6.4	8.1	5.2	6.8	8.5	8.9
NO _x , ppb	API	36.7	24.3	32.8	23.6	25.6	19.8	16.0	10.5	9.7	10.6	12.9	14.6	19.9
NO ₂ , ppb	API	18.7	14.9	16.6	16.7	17.0	13.2	12.2	8.9	8.1	8.6	9.8	9.9	12.9
O ₃ , ppb	API	16.4	21.9	13.5	19.2	23.9	28.1	31.1	39.1	39.5	31.0	24.8	19.8	25.7

^a Includes only the data when both TEOM and FRM data were available.

^b Organic material obtained from the carbon evolved below 340EC, assuming the organic material is 63% carbon.

^c Elemental carbon (soot) obtained from the carbon evolved above 340EC.

Acknowledgement The authors would like to acknowledge Elias J. George for his assistance in purchasing the TEOM and FRM samplers.

Disclaimer

Reference in this report to any specific commercial product, process, or service is to facilitate understanding and does not necessarily imply its endorsement or favoring by the United States Department of Energy.

References

- (1) US EPA (1998) "Quality assurance guidance document method compendium: PM_{2.5} mass weighing laboratory standard operating procedures for the performance evaluation program," US Environmental Protection Agency Office of Quality Planning and Standards, Research Triangle Park, NC 2771, 1998.

NEW METHOD FOR MEASURING THE GRAPHITE CONTENT OF ANTHRACITE COALS AND SOOTS

Yi Jin Jiang, Mark S. Solum, Ronald J. Pugmire,*
and David M. Grant

Department of Chemistry, University of Utah,
Salt Lake City, Utah 84112

Harold H. Schobert and Peter J. Pappano

The Energy Institute, The Pennsylvania State University,
University Park, PA 16802

Introduction

The amount of graphite-like structure of anthracitic coals and soots is an important parameter for understanding the composition of these materials. The structure of graphite has been studied extensively¹⁻⁶, and is described by the delocalization of the π electrons over the carbon structure. These delocalized π electrons contribute to the conductivity of graphitic material. A recently proposed structure of coals⁷ and soots consists of regions or clusters that are graphite-like in nature, linked by non-conductive chain/bridging regions. The electrical conductivity of these materials will therefore depend on the extent of these graphitic regions. Therefore, by measuring the electrical conductivity of these samples it is possible to estimate the amount of graphitic materials present.

The direct measurement of electrical conductivity is a classical method⁸ in which a pair of electrodes is placed across the sample. However, due to the low resistivity (1.5×10^{-3} ohm-cm),⁹ the resistance of the electrical contact between the electrodes and the sample could seriously affect the measurement results, especially when the sample is a powder. In addition, the heterogeneity of the samples and the presence of nonconductive regions make it difficult to measure the electrical conductivity of the sample in this manner. In order to solve such problems, the method of measuring the quality factor (Q value) of a radio frequency (RF) coil at high frequency has been employed.^{10,11}

A Q meter is used to measure the Q value of a RF coil which is defined by:

$$Q = 2\pi fL/R \quad (1)$$

where, f is the applied frequency, R is the resistance of the coil at this frequency, and L is the inductance of the coil. When a sample is placed inside the coil, any conduction electrons in the sample will be driven into motion by the electric field induced by the high frequency magnetic field inside the coil according to the Faraday Law¹².

$$\nabla \times E = -\partial B / \partial t. \quad (2)$$

The interaction of moving electrons with the graphite lattice leads to an energy loss. This energy loss inside a coil results in a decrease in the Q value of the coil and therefore a resultant increase in resistance. The ΔQ between an empty and a sample filled coil is directly proportional to ΔR . Since ΔR is a measure of the delocalized electron content, it is also a reflection of the graphitic carbon content of the sample.

Experimentally, the correlation between ΔQ and the graphitic carbon content can be obtained by performing the measurement on a series of standard samples where pure graphite is diluted with silica gel of known composition. The graphitic carbons content in the unknown sample, i.e., the coal or soot, can then be estimated by determining ΔQ on a sample of known mass.

The Principle of the Measurement

The Q value of an RF coil is measured with a Q meter, a classical electrical instrument.¹³ Let Q_0 be the value of the empty coil. The value of Q_0 decreases to Q_i when a sample that contains conductive material is placed inside the coil, but the inductance L remains essentially the same (less than 1% change). The energy loss due to the moving conduction electrons interacting with the graphite lattice causes an increase in the resistance from R to $R + \Delta R$ with a corresponding decrease in the quality factor from Q_0 to Q_i and

$$Q_i = 2\pi fL / (R + \Delta R). \quad (3)$$

Equation 3 can be rewritten as

$$Q_i = 2\pi fL / R(1 + \Delta R/R) = Q_0 / (1 + \Delta R/R) \quad (4)$$

For the coil used in this study at $f = 100$ MHz, $Q_0 = 258$, $L = 0.145 \mu\text{H}$ and the calculated value of R is 0.353Ω . Substituting these data into equation 4 gives:

$$Q_i = 258 / (1 + \Delta R / 0.353 \Omega) = 258 / (1 + \Delta R 2.83 \Omega^{-1}) \quad (5)$$

A plot Q_i vs ΔR results in a hyperbolic curve with a vertical asymptote at $\Delta R = -0.353 \Omega$. Inverting both sides of equation 5 yields the linear relationship:

$$1/Q_i = (1 + \Delta R 2.83 \Omega^{-1}) / 258 = 0.00388 + \Delta R 0.011 \Omega^{-1} \quad (6)$$

Recognizing that ΔR is much less than 1Ω a Taylor series expansion ($1/(1+x) \cong 1-x$) yields equation 7:

$$Q_i = 258(1 - \Delta R 2.83 \Omega^{-1}) \quad (7)$$

As mentioned earlier ΔR is proportional to the G , the quantity of graphite (mg) in this limited volume of sample. Therefore, G can be represented by:

$$G = K \Delta R \quad (8)$$

By obtaining a series of Q_i and ΔR values from a set of samples with known graphite concentration the coefficient K can be obtained and a linear relationship between Q_i and G can be written as:

$$Q_i = 258[1 - (G/K) 2.83 \Omega^{-1}] \quad (9)$$

which can be rearranged to:

$$G = -1.37 \times 10^{-3} Q_i K \Omega + 0.353 K \Omega \quad (10)$$

The practical form of equation 10 will be discussed in the next section.

Experimental Details

A Q meter (Type 170A, Boonton Radio Corporation U. S. A.) was used for measuring the Q value of a RF coil. The operating frequency was 100MHz for reasons of convenience, coil size and Q measurement sensitivity. A five-turn solenoid coil of inside diameter 0.83 cm, and length 1.40 cm, wound from 16-swg copper wire was used for the experiments. The inductance of this solenoid coil is $0.145 \mu\text{H}$ and at 100MHz the Q value is 258.

Each sample was placed in a zirconia solid-state rotor (Chemagnetics, Inc.). In each measurement a constant volume of sample (0.33 cm^3) was used which filled to solenoid. A set of standard samples was prepared by mixing pure graphite powder (Aldrich Catalogue NO: 28286-3) with silica gel (Aldrich Catalogue NO: 28859-4). The value of Q_i is silica gel independent. The standard and test samples occupied the same volume. Care was taken to place the sample in the sample holder such that the entire sample was within the coil for the Q measurement. The mass of each sample was also recorded.

The measurements of the unpaired electron concentration in each sample were made on a Bruker ESR spectrometer. Experimental details of the measurement will be discussed in a subsequent paper. All NMR measurements were obtained on a Chemagnetics CMX-100 spectrometer using a PENCIL rotor spinning system under conditions described previously.¹⁴ All experiments were carried out at room temperature.

* To whom correspondence should be addressed

Results and Discussion

Table 1 contains the Q_i values associated with the standard samples of varying graphite content. The least squares fit of the data is:

$$G \text{ (mg)} = -0.69917Q_i + 182.30 \quad (11)$$

This is the form of equation (10) and is used to calculate the graphite content of test samples. The graphite factors in Tables 3 and 4 are the values derived from equation 11 normalized by the weight of the sample.

Four anthracitic coals (LCNN, Jeddo, UAE and Summit) obtained from The Pennsylvania State University were used in this study. The elemental analysis is provided in Table 2. The measured Q_i values, the graphite content, the atomic ratios C/H and the concentration of the unpaired electrons are given in Table 3. Similar information for several soot samples is given in Table 4.

This method has been applied for the first time to measure the graphite-like structures in the anthracites and soot samples. Both of these materials are of complex composition containing mixtures of both amorphous and semi-ordered structures and, as far as the investigators can determine, no data of this type have previously appeared in the literature. However, based on some results from other experiments, a possible qualitative explanation will be discussed as below.

The data in Table 3 indicate that the differences in graphitic carbon content of the four anthracites is significant, i. e., by an order of magnitude when one compares the data of the LCNN and Summit samples. However, the concentration of unpaired electrons in these four samples is essentially constant, varying by less than a factor of 2. The graphite factor in the anthracite sample with the highest concentration of unpaired electrons (UAE) is only 0.024. These results indicate that not all measured unpaired electrons contribute to the electrical conductivity. No change in the Q value of a coil is observed when a stable free radical such as DPPH (a standard free radical sample) is placed in the coil. These data indicate that there are at least two different types of electrons in the systems under study; 1) electrons such as found in DPPH where the electron is localized and, 2) electrons that can occupy conduction bands in graphite type structures made up of extended hexagonal ring systems. These extended ring systems may contain, especially in the soot samples, some five-member rings.¹⁵

It is still not clear what size hexagonal ring systems is large enough to exhibit conduction behavior. For example, coronene, which has seven rings, has no effect on the Q value of the RF coil. Celzard⁷ proposed that at least 70 hexagonal rings and a C/H weight ratio higher than 50 (atomic C/H \approx 4.2) is where conductive behavior starts. According to the data shown in Table 3 the atomic C/H ratio of the anthracite coals from LCNN to Summit is 5.35, 4.44, 3.59, and 3.13, respectively. Comparison of these data with the graphitic carbon content seems to be reasonably in line with the results of Celzard.

The ¹³C MAS spectra of four of the samples examined in this study are shown in Figure 1. The spectra of two anthracites and the anthracene soot residue were obtained using the CP technique. The diesel soot spectrum was taken with the single pulse technique due to a depletion of protons in the sample which renders the CP technique ineffective. These four samples have quite different percentages of the graphitic carbon. The graphite-factors for the four samples are: 0.014, 0.148, 0.48 and 0.61 for Summit, LCNN, the 1400 K anthracene soot residue and diesel soot #4, respectively. One can see that there is a great variation of line widths among the four samples that, to some degree, follows the graphite factor. The increased line width is due to anisotropy of the magnetic susceptibility of regions of graphene layering that is not totally removed under MAS

conditions.^{16,17} The Summit sample has the appearance of a normal diamagnetic sample with a very small graphite factor and no unusual line broadening. While the line width (FWHM) of the LCNN is essentially the same as that of the Summit, some line broadening appearing as Lorentzian are evident in the LCNN sample. The anthracene soot residue has even broader wings and the broadening of the main resonance is approximately 40% than that of the LCNN. The diesel engine soot has an extremely broad resonance, which is also noted in samples so deficient in proton content that the CP experiment is not effective.¹⁴

Conclusion

A rather simple method seems to be useful for correlating sample conductivity with the presence of graphene layering in graphitic carbon structures in anthracitic coals and numerous soot samples. The technique reported is useful for estimating the amount of graphite like structures in amorphous carbonaceous samples. It has been demonstrated that the number of unpaired electrons, per se, may not be a reliable parameter for estimating either sample conductivity or the extent of graphitization of soot samples. By utilizing a radio frequency coil one can induce a high frequency electric field in the sample and thus avoid any physical contact with the sample. This technique renders the experimental results free from any of the classical problems associated with electrical contact at the surface. The data indicate that the concentration of free radicals in the sample is not a reliable indication of either the conductivity of the sample or the amount of graphitic carbon present. High resolution TEM data indicate that different levels of ordered structures exist in many of the samples that we have examined and an analysis of the relationship between structure and conductivity will be attempted.

Acknowledgments. The University of Utah gratefully acknowledges the support by the Department of Energy as part of the Advanced Strategic Computing Program through contract number B341493 from Lawrence Livermore National Laboratory, DOE Fossil Energy/National Petroleum Technology Office contract No. DE-AC 26-99BC, DOE/National Energy Technology Laboratory through the Consortium for Fossil Fuel Liquefaction Sciences (through the University of Kentucky, Lexington), the National Science Foundation under NSF CRAEMS grant CHE 0089133, and by The Consortium for Premium Carbon Products from Coal at The Pennsylvania State University.

Table 1. The Q_i value associated the samples with different graphite content.

Sample	Sample Weight (mg)	Graphite Content (mg)	Graphite (%)	Q_i Value ^a
1	181.9	60.3	33.2	182.4
2	185.2	36.5	19.7	199.2
3	167.3	24.2	14.5	222.0
4	177.6	17.2	9.68	242.2
5	182.7	8.6	4.7	248.2
6	193.2	5.8	3.0	252.0
7	193.0	4.2	2.2	254.4

a) The frequency of the measurement was 100MHZ; at this frequency the Q value of the empty coil is 258.

Table 2. Elemental analyses of the anthracite coal samples.

Sample	C (%)	H (%)	N (%)	S (%)	O (%) (by diff)
LCNN	95.7	1.5	1.2	0.5	1.0
Jeddo	95.2	1.8	1.1	0.6	1.3
UAE	94.0	2.2	1.0	0.5	2.3
Summit	93.2	2.5	1.6	0.6	2.2

Table 3. The measured graphite-factor, C/H atomic and mass ratios, Q_i measurement, and spin concentration of unpaired electrons of the anthracite coal samples.

Sample	Graphite Factor	Atomic C/H	C/H Weight Ratio	Q_i Value ^a	Spin Concentration (10^{19} spins/g)
LCNN	0.148	5.35	63.8	184	3.3
Jeddo	0.112	4.44	52.9	200	3.5
UAE	0.024	3.59	42.7	250	4.9
Summit	0.014	3.13	37.3	254	2.6

a) The frequency of the measurement was 100MHz; at this frequency the Q value of the empty coil is 258.

Table 4. The measured graphite-factor and unpaired electron spin concentration of some soot samples.

Sample	Sample Weight (mg)	Graphite Factor	Q_i Value ^a	Spin Concentration (10^{19} spins/g)
Anthracene 1400 K Soot Residue	163	0.48	148.8	11.00
Diesel Soot Residue ^b	192	0.43	143.0	0.87
Ethylene Soot Residue ^b	150	0.48	157.0	3.78
NIST DPM 1650 Residue ^b	180	0.34	172.0	1.11
Diesel Soot #1	174	0.47	141.0	3.99
Diesel Soot #3	177	0.28	150.0	3.60
Diesel Soot #4	186	0.61	123.0	3.82
Diesel Soot #5	186	0.61	124.0	3.00

a) The frequency of the measurement was 100MHz; at this frequency the Q value of the empty coil is 258.

b) Residue is the insoluble part after 24 hrs extraction with dichloromethane in a Soxhlet extraction system.

References

- Mantell, C. L., Carbon and Graphite Handbook; Interscience Publishers: New York, 1968, pp. 6-43.
- Wallace, P. R., *Phys. Rev.*, 1947, 71, 622.
- Schobert, H. H., The Chemistry of Hydrocarbon Fuels; Butterworths: London, 1990, pp. 293-295.
- McClure, J. W., *Phys. Rev.*, 1956, 104, 666.
- Wagoner, G., *Phys. Rev.* 1960, 118, 647.

- Singer, L.S., Wagoner, G., In Proc. Fifth Carbon Conf; Pergamon Press: New York, 1963, pp. 65-71.
- Celzard, A., Mareche, J. F., Payot, F., Begin, D., Furdin, G., *Carbon*, 2000, 38, 1207.
- Terman, F. E., Radio Engineer's Handbook, 1st. ed; McGraw-Hill: New York, 1943, pp. 26-47.
- Tyler, W. W., Wilson Jr., A. C., *Phys. Rev.* 1953, 89, 870.
- Terman, F. E., Radio Engineer's Handbook, 1st. ed; McGraw-Hill: New York, 1943, pp. 74-83.
- Jiang, Y. J., *J. Magn. Reson.*, 2000, 142, 386.
- Hayt Jr, W. H., Engineering Electromagnetics; McGraw-Hill Book Company: New York, 1981, pp. 346-353.
- Terman, F. E., Radio Engineer's Handbook; 1st. ed; McGraw-Hill: New York, 1943, p. 916.
- Solum, M. S., Sarofim, A. F., Pugmire, R. J., Fletcher, T. H., Zhang, H., *Energy Fuels*, 2001, 15, 961.
- Orendt, A. M., Facelli, J. C., Bai, S., Rai, A., Gossett, M., Scott, L., Boerio-Goates, J., Pugmire, R. J., Grant, D. M., *J. Phys. Chem. A*, 2000, 104, 149.
- Kume, K., Hiroshima, Y., *Solid State Commun.*, 1988, 65, 617.
- Freitas, J. C. C., Emmerich, F. G., Cernicchiaro, G. R. C., Sampaio, L. C., Bonagamba, T. J., *Solid State NMR*, 2001, 20, 61.

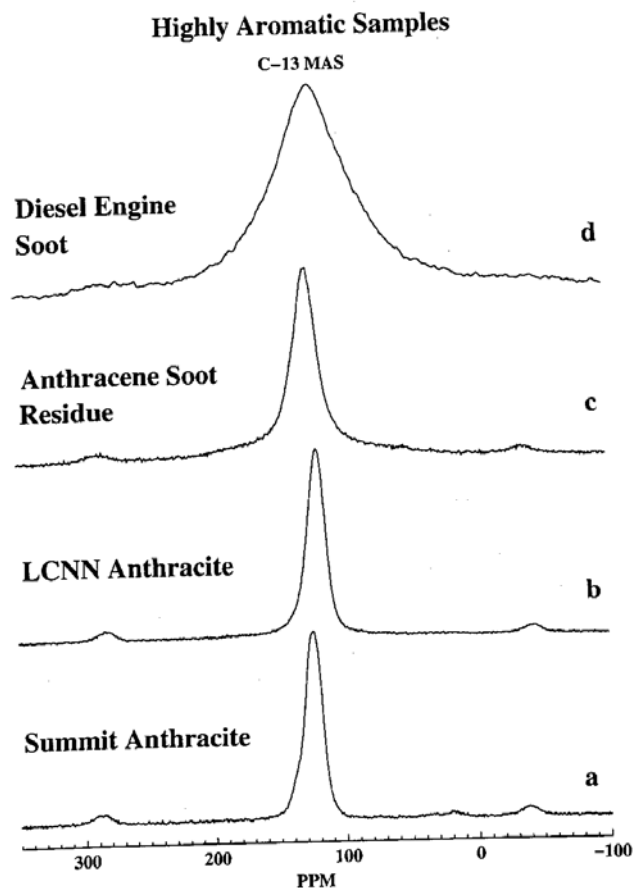


Figure 1. ^{13}C MAS spectra of four of the samples. The spectra in a, b, c were taken with the CP technique all with a 1 s pulse delay. a) 3 ms contact time b) 10 ms contact time, c) 10 ms contact time d) spectrum taken with the single pulse method and using a 10 s pulse delay.

NO_x REDUCTION OVER PROMOTED CARBON SYSTEMS

J.M. Calo and D. Lopez
Chemical Engineering Program
Division of Engineering
Brown University
Providence, RI 02912

Introduction

Promoted carbons offer some potentially significant advantages for heterogeneous NO_x reduction. These include: low cost; high activity at low temperatures, which minimizes carbon loss and improves oxygen resistance; and a support material that can be engineered with respect to porosity, transport and catalyst dispersion characteristics. In addition, it is known that certain gases, such as NH₃, CO, and H₂, can act as reducing agents for NO in carbonaceous systems in which carbon behaves somewhat like a heterogeneous catalyst. Thus, depending on the specific nature of the carbonaceous material and the operating conditions, carbon can simultaneously behave like a reactant, a catalyst, and a catalyst support. In the current work, results on the role of CO as a reducing agent and the effects of a catalyst (potassium) are reported.

Experimental

Reactivity measurements were conducted in a quartz, packed bed reactor/gas flow system. Gas concentrations up to 4000 ppm of NO, N₂O, and CO in helium were used. A NO_x chemiluminescence analyzer, a quadrupole mass spectrometer (QMS), and a dual-column gas chromatograph were used for gas composition analyses.

Approximately 100 mg of phenol-formaldehyde resin char, produced from the same batch of resin was used for each run. The char was promoted with potassium by immersion in potassium acetate (0.5M) at 60°C for 4h. The resultant material was washed with distilled water until no potassium was detected in the filtrate. The final potassium content of the char was determined by extraction in 1M HCl for 8h. Analysis by atomic absorption indicated a potassium content of 2.03% by weight.

Char samples were thermally cleaned at 950°C for two hours prior to each run. They were then reacted isothermally in the selected gas mixture at atmospheric pressure to pseudo-steady-state conditions. At the end of the reaction run, the sample was allowed to quench rapidly in helium by shutting off the furnace power and moving the furnace laterally off the packed bed. After cooling to 300K, temperature programmed desorption (TPD) of the surface complexes was performed at 20K/min in helium to approximately 1273K, while monitoring the gas phase composition.

Results and Discussion

NO Reduction. A summary of reactivity data is presented in Figure 1. As shown, in the presence of just NO, the apparent activation energy over the unpromoted char is *ca.* 180 ± 10 kJ/mol at temperatures > 923K. In the presence of additional CO, however, the reactivity increased (by about a factor of 8 at 923K), and the apparent activation energy decreased to about 97 ± 10 kJ/mol. In the presence of potassium, the reactivity increased again to a total of about a factor of two at the highest temperature, to 10 at the lowest temperature, in comparison to that for the unpromoted char in the absence of additional CO. The presence of potassium decreased the apparent activation energy to 89 and 85 ± 9 kJ/mol, for the 2000 and 4000 ppm NO cases, respectively. Thus, the presence of potassium catalyzes the NO-carbon reaction both by increasing the number of active sites and/or the turnover rate on these sites, as well as by

significantly decreasing the apparent activation energy. Illán-Gómez *et. al.*¹ reported an activation energy ranging between 30 and 86 kJ/mol in the low temperature regime (300-600°C) for the NO-carbon reaction in the presence of various metal catalysts. The apparent activation energy reported here agrees with that found at the highest temperatures in that work. It was also found that whenever there is enhancement of reactivity due to catalysis by potassium or CO, the CO/CO₂ product ratio decreases; i.e., there is enhanced CO₂ production. The reactivity is close to first order in NO for both the unpromoted and potassium-promoted char (e.g., see the 2000 and 4000 ppm data for the potassium-promoted char presented in Figure 1). This is consistent with our earlier work on unpromoted char.²

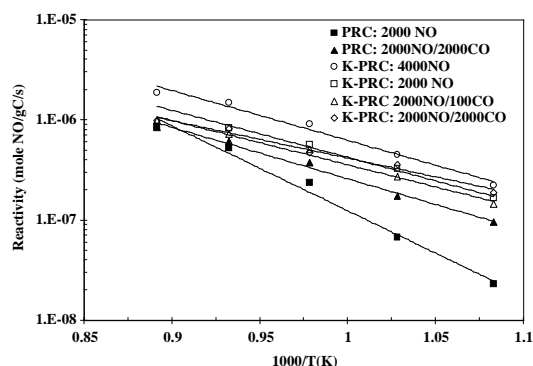


Figure 1. Arrhenius plots for unpromoted (PRC) and potassium-promoted (K-PRC) phenolic resin char, with and without additional CO in the feed gas.

Desorption spectra of CO and CO₂ from the char samples following steady-state reaction indicated that there were considerably more oxygen surface complexes of all types produced on the potassium-promoted char than the unpromoted char (~6X @ 800°C), and that this relative discrepancy increased with decreasing temperature (~12X @ 650°C), although the total amount of oxygen surface complexes also decreased (but more slowly) with decreasing temperature for the potassium-promoted char. This is consistent with the preceding observation that catalysis by potassium increases in relative effectiveness with decreasing temperature.

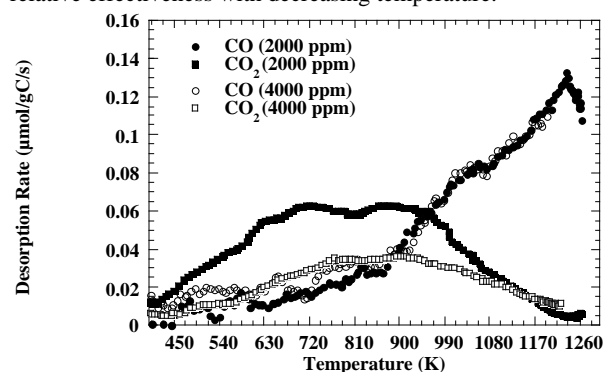


Figure 2. CO and CO₂ desorption rates from potassium-promoted phenolic resin char following reaction in 2000 ppm and 4000 ppm NO at 800°C.

Sample TPD spectra from the potassium-promoted char are presented in Figure 2. As shown, under these conditions, the NO concentration affects the surface population of CO₂-producing complexes much more than the CO-producing complexes, such that the population of the former *decreases* with increasing NO concentration. This effect was noted at all temperatures, except that at lower temperatures the population of CO-producing complexes starts to decrease with increasing NO concentration as well. A

mechanism has been formulated that explains this behavior by incorporating the mechanistic steps:



The former has been proposed in the literature,³ and the latter is based on our work.

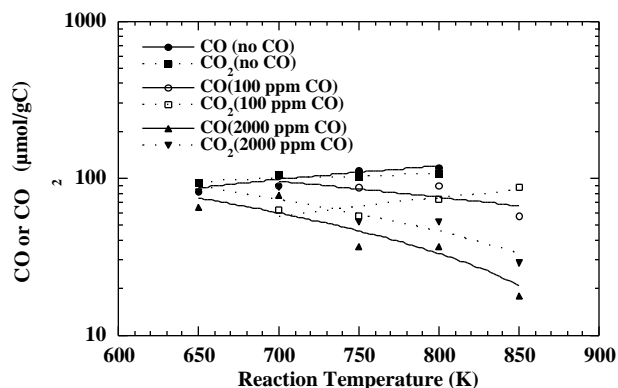


Figure 3. Post-reaction CO and CO₂ desorption yields from potassium-promoted resin char following reaction in 2000 ppm NO and the indicated amounts of additional CO, as a function of reaction temperature.

The effect of additional CO in the gas phase for the promoted char is summarized in Figure 3. As shown, in the case of no added CO, both CO and CO₂ desorption yields *increase* with increasing reaction temperature. The addition of 100 ppm CO, alters this trend and causes both desorption yields to remain practically constant or decrease slightly with reaction temperature. The addition of 2000 ppm CO causes the desorption yields of both CO and CO₂ to *decrease* significantly with reaction temperature. Thus, it is clear that relatively large amounts of CO cause a significant depletion in the population of oxygen surface complexes, in comparison to reaction in just NO. However, as shown in Figure 1, the NO reduction reactivity on the potassium-promoted resin char appears to become less sensitive to the additional CO, with increasing reaction temperature. In addition, it has been established that the reactivity continues to scale approximately as NO concentration.

In its simplest form, the mechanism of NO reduction on a metal-promoted carbon can be separated into two major processes – oxygen surface complex formation and desorption. In turn, oxygen surface complex formation also occurs *via* two major processes: (1) the redox process on the metal catalyst sites; e.g., NO oxidation of potassium and reduction by carbon; and (2) non-catalytic NO chemisorption/oxidation of active carbon sites.³ Although both processes occur in parallel, in the presence of an active metal catalyst the redox process generally appears to be the dominant mechanism. In this context, the following mechanistic hypotheses seem to reconcile our observations. At low reaction temperatures, the desorption behavior of the oxygen surface complexes controls the overall reduction reactivity. That is, the redox cycle on the potassium metal sites is sufficiently rapid to produce oxidized carbon sites as rapidly as they are depopulated due to thermal desorption. With increasing temperature, however, the desorption rate becomes sufficiently rapid such that the rate-limiting process becomes the rate of reaction with potassium metal sites. Additional CO in the gas phase does not appear to interfere with the catalytic oxidation process. Since the latter controls the rate only at high temperatures, the additional CO increases the reactivity only at low temperatures, and then primarily *via* the action of more labile C(CO) complexes formed from CO *via*:⁴



Since these latter complexes are labile, additional CO can only have a significant effect on reactivity under conditions where a large population of C(CO) can be sustained; i.e., at low temperatures and high gas phase CO concentrations.

N₂O Reduction. N₂O reduction on the potassium-promoted resin char exhibited a lower apparent activation energy (65 ± 7 kJ/mol) than NO reduction over the same material. This is attributed to the weaker N-O bond energy in N₂O.

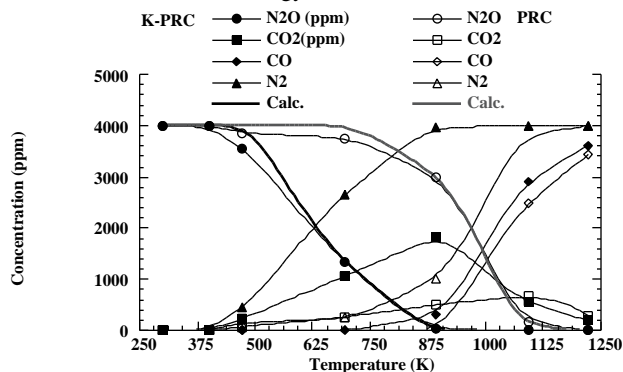


Figure 4. Temperature programmed reaction (TPR) at 20K/min in 4000 ppm N₂O over potassium-promoted (closed) and unpromoted (open) resin char.

The results of two TPR experiments are presented in Figure 4. As shown, N₂O reduction over the potassium-promoted char begins at about 200°C, while appreciable NO reduction begins at much higher temperatures. N₂O reduction over the potassium-promoted resin char produces primarily CO₂ and hardly any CO. (The CO produced at high temperatures for the unpromoted char is attributed to CO₂ gasification.) The fit curves for N₂O consumption were calculated assuming the experimentally-determined apparent reaction orders of $n = 1$ over the potassium-promoted resin char, and $n = 0$ over the unpromoted resin char. This behavior is attributed to the fact that the reaction appears to be controlled by surface complex formation catalyzed by metallic sites in the promoted char, and oxygen surface complex desorption in the unpromoted char.

The effect of additional CO in the feed gas was to increase CO₂ evolution considerably, while not having any discernible effect on the N₂O reduction rate. This behavior is attributed to the formation of C(CO) complexes by CO, which then react further with CO to desorb CO₂ and deposit carbon on the surface. The C(CO) complexes are thought to be similar to those hypothesized for NO reduction in the presence of additional CO. However, unlike NO, which apparently does react with these complexes, resulting in the “catalytic effect” of CO, N₂O does not seem to react with them; only CO does, apparently *via* the Boudouard reaction.

Acknowledgment

This work was supported by the University Coal Research Program of the National Energy Technology Laboratory of the U.S. Department of Energy under Grant No. DE-FG26-97PC97267. D.L. would like to thank Fulbright-Colciencias for a partial fellowship.

References

- Illán-Gómez, M. J., Linares-Solano, A., Radovic, L.R., and Salinas-Martínez de Lecea, *Energy & Fuels*, 1995; 9: 983.
- Suuberg, E.M., Teng, H., and Calo, J.M., *23rd Symp. (Int.) Comb.* 1990: 1199-1205.
- Li, Y. H., Lu, G. Q., Rudolph, V., *Chem. Eng. Sci.*; 1998; 53:1.
- Calo, J.M., Lopez, D., Burnett, A., Aarna, I., and Suuberg, E.M., Paper No. 6.1, *Proc. Carbon '01*, Lexington, KY, 2001.

SEWAGE SLUDGE DERIVED MATERIALS AS ADSORBENTS OF ACIDIC GASES

Andrey Bagreev, Svetlana Bashkova, and Teresa J. Bandosz

Department of Chemistry, the City College of New York and the Graduate School of the City University of New York, 138th street and Convent Ave, New York, NY 10031; e-mail: tbandosz@ccny.cuny.edu

Introduction

The process of carbonization of biosolids has been studied in detail using different chemical agents and various conditions [1-11]. Materials obtained as a result of the treatment have surface areas between 100 and 500 m²/g, but their performance as adsorbents has been demonstrated to be much worse than that of activated carbons. The ability of these adsorbents to remove organics such as phenols, or sulfur dioxide and hydrogen sulfide [10, 11] have been tested so far; their capacity for the adsorption of SO₂ reported by Lu was less than 10% of the capacity of Ajax activated carbon [11]. When the performance for H₂S adsorption was compared, the capacity of sludge-derived adsorbents was only 25% of the capacity of Calgon carbon, IVP 4x6 [10].

The objective of this paper is to demonstrate the superior performance of materials obtained by simple carbonization of the New York City municipal sewage sludge-derived product, Terrene[®], as adsorbents for hydrogen sulfide and sulfur dioxide. The results obtained show that the capacity of these adsorbents exceeds that of coconut shell-based activated carbon, which is considered as one of the alternative sorbents to replace the caustic-impregnated carbons commonly used as hydrogen sulfide adsorbents in municipal sewage treatment plants [13, 14].

Experimental

Materials. Terrene[®] was obtained from the New York Organic Fertilizer Company (Bronx, New York) in the form of 3 mm diameter granules with about 5% water content. The detailed chemical composition is presented [12]. The adsorbents studied were prepared by pyrolysis of Terrene[®] at temperatures between 673 – 1223 K in a nitrogen atmosphere in a fixed bed (horizontal furnace). The samples are referred to as SC-1, SC-2, SC-3 and SC-4 where last digits represent the pyrolysis temperatures of 673, 873, 1073 and 1223 K, respectively.

For comparison, the experiments were done using the as-received carbon manufactured from coconut shells by Watelink Barnabey and Sutcliffe, S208. The prepared materials were studied as hydrogen sulfide adsorbents in the dynamic tests described below. After exhaustion of its adsorbent capacity either for H₂S or SO₂ adsorption, each sample is identified by adding the letter “E” to its designation.

Methods. The dynamic tests were carried out at room temperature to evaluate the capacity of sorbents for H₂S and SO₂ removal [15, 16]. Adsorbent samples were packed into a column (length 60 mm, diameter 9 mm, bed volume 6 cm³) and prehumidified with moist air (relative humidity 80 % at 25 °C) for an hour. The amount of adsorbed water was estimated from the increase in the sample weight. Moist air (relative humidity 80 % at 25 °C) containing 0.3 % (3000 ppm) H₂S or SO₂ was then passed through the column of adsorbent at 0.5 L/min. The elution of H₂S was monitored using an Interscan LD-17 H₂S continuous monitor system interfaced with a computer data acquisition program. SO₂ concentration was monitored using Lumidor electrochemical

sensor. The test was stopped at the breakthrough concentration of 500 ppm for H₂S and 350 ppm for SO₂. The adsorption capacities of each sorbent in terms of milligrams of H₂S or SO₂ per gram of carbon were calculated by integration of the area above the breakthrough curves, and from the H₂S and SO₂ concentration in the inlet gas, flow rate, breakthrough time, and mass of sorbent.

Nitrogen adsorption isotherms were measured using an ASAP 2010 analyzer (Micromeritics, Norcross, GA, USA) at 77K. Before the experiment the samples were degassed at 393K to constant pressure of 10⁻⁵ torr. The isotherms were used to calculate the specific surface area, S_{N2}; micropore volume, V_{mic} and total pore volume, V_t. All the parameters were determined using Density Functional Theory (DFT) [17].

To evaluate the surface pH a 0.4 g sample of dry adsorbent was added to 20 mL of deionized water and the suspension stirred overnight to reach equilibrium. The sample was filtered and the pH of solution was measured using an Accumet Basic pH meter (Fisher Scientific, Springfield, NJ, USA).

Thermal analysis was carried out using TA Instruments Thermal Analyzer (New Castle, DE, USA). The heating rate was 10 deg/min in a nitrogen atmosphere at 100 mL/min flow rate.

Results and Discussion

The breakthrough curves for our samples are shown in Figures 1 and 2. For comparison, the curves obtained for coconut shell-based activated carbon, are included. The calculated capacities are summarized in Table 1. It is clearly seen that with increasing pyrolysis temperature the capacity of the sludge-derived adsorbents is significantly increased. It is remarkable that the H₂S breakthrough capacity of the sample treated at 1223 K, SC-4, is twice that of the as received activated carbon.

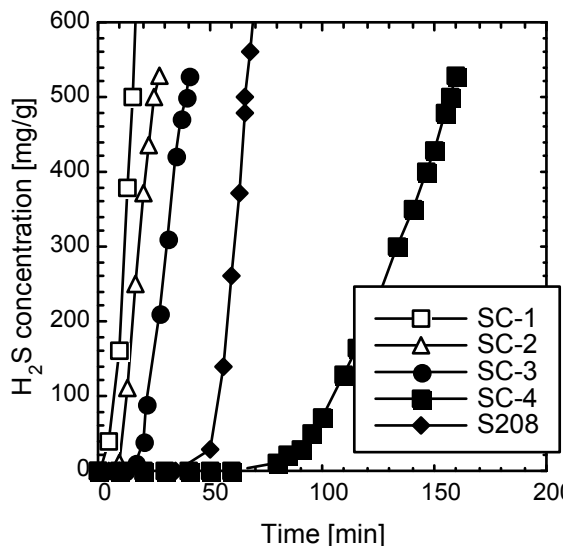


Figure 1. H₂S breakthrough curves.

As indicated elsewhere [14, 18, 19], the presence of water on activated carbons enhances the dissociation of hydrogen sulfide and facilitates to its oxidation to sulfur and sulfur dioxide. In the case of the sludge-derived materials, the mechanism of hydrogen sulfide removal probably differs from that for activated carbons. For the activated carbons, the significant decrease in the adsorption capacity corresponding to exhaustion is usually caused by the formation of sulfuric acid [14, 19]. For the sludge-derived samples, only a small decrease in pH is observed and after exhaustion the materials preserve their basic pH. As was pointed out elsewhere [14, 18, 19],

for conventional carbons, basic/neutral initial pH favors the formation of elemental and polymeric sulfur as the final products of oxidation; there is a threshold pH below which this process becomes infeasible. However, this rule probably does not apply to our sludge-derived materials. The high capacity is probably caused by the catalytic effect of inorganic matter [15, 16, 20]. The possibility of chemisorption in the process of H₂S removal on sludge-derived carbon was also pointed out by Lu and Lou; however, the capacity of their adsorbent was reported to be only 25% of that of activated carbon chosen for a comparison [10]. A remarkably good performance of the SC-4 carbon as a hydrogen sulfide adsorbent also indicates that differences in the mechanisms of the process exist within the series of materials, probably attributable to changes in their chemical and structural composition.

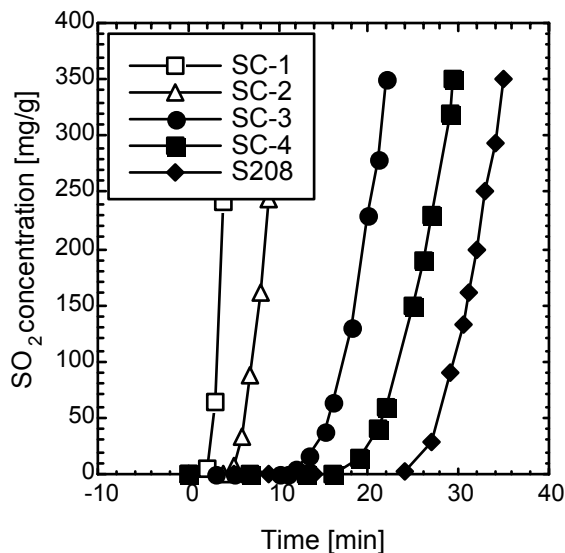


Figure 2. SO₂ breakthrough curves.

Table 1. pH of the materials studied, their H₂S and SO₂ breakthrough capacities, and the quantity of water adsorbed during prehumidification (pH_{H₂S}/pH_{SO₂} – pH values for exhausted samples after H₂S and SO₂ adsorption experiments)

Sample	pH pH _{H₂S} / pH _{SO₂}	H ₂ S breakth. capacity (mg/g)	SO ₂ breakth. capacity (mg/g)	Water ads. (mg/g)
SC-1	7.9	8.2	5.1	60
SC-1E	7.5/6.7	---	---	---
SC-2	11.4	14.9	9.5	40
SC-2E	9.2/8.8	---	---	---
SC-3	11.2	23.6	22.2	48
SC-3E	8.8/8.5	---	---	---
SC-4	10.8	82.6	29.8	62
SC-4E	9.9/7.1	---	---	---
S208C	10	48.8	48.2	77
S208CE	7.4/2.2	---	---	---

Structural parameters calculated from nitrogen adsorption isotherms are given in Table 2. As discussed elsewhere [12], the surface area and pore volumes increase with increasing carbonization temperature. It is noteworthy that there are no significant differences in the porosity of SC-3 and SC-4, which could explain the differences in their H₂S and SO₂ adsorption capacities. This supports

our hypothesis that significant changes in surface chemistry favorable to H₂S and SO₂ chemisorption occur when the sludge is pyrolyzed at 1223 K. After H₂S and SO₂ adsorption/oxidation, the surface areas and pore volumes significantly decreased. This decrease is especially apparent in the volume of micropores indicating that they are active in the adsorption/oxidation process.

The study of adsorption products using thermal analysis showed that elemental sulfur and metal sulfides are the main products of surface reactions[15, 16].

Table 2. Structural parameters calculated from nitrogen adsorption isotherms. For exhausted samples the data for H₂S (first number) and SO₂ (second number) experiments is reported.

Sample	S _{N₂} (m ² /g)	V _{mic} (DFT) (cm ³ /g)	V _t (0.995) (cm ³ /g)
SC-1	21	0.006	0.075
SC-1E	8/7	0.003/0.003	0.057/0.055
SC-2	92	0.030	0.115
SC-2E	9/8	0.001/0.003	0.040/0.049
SC-3	106	0.033	0.107
SC-3E	9/27	0.003/0.008	0.064/0.056
SC-4	104	0.028	0.100
SC-4E	13/32	0.002/0.007	0.065/0.053
S208	889	0.359	0.457
S208E	774/690	0.352/0.280	0.414/0.296

Conclusions

The results presented in this paper demonstrate that sewage-sludge derived materials can work efficiently as adsorbents for H₂S and SO₂ from moist air. The reaction proceeds until the all pore volume is filled with the oxidation products.

References

- (1) Manahan, S.E. *Environmental Chemistry*, 6th ed.; CRC Press: Boca Raton, FL, 1994.
- (2) Biosolid Generation, Use, and Disposal in TheUnited States: EPA530-R-99-009, September 1999; www.epa.gov.
- (3) Sutherland, J. US Patent 3,998,757 (1976).
- (4) Nickerson, R.D.; Messman, H.C. US Patent. 3,887,461 (1975)
- (5) Lewis, F. M. US Patent 4,122,036 (1977).
- (6) Kemmer, F.N.; Robertson, R.S.; Mattix, R. D. US Patent 3,619,420 (1971)
- (7) Abe, H.; Kondoh, T.; Fukuda, H.; Takahashi, M.; Aoyama, T.; Miyake, M. US Patent 5,338,462 (1994).
- (8) Chiang, P.C.; You, J.H. *Can. J. Chem. Eng.* **1987**, *65*, 922.
- (9) Lu, G.Q.; Low, J.C.F.; Liu, C.Y.; Lau, A.C. *Fuel* **1995**, *74*, 3444.
- (10) Lu, G.Q.; Lau, D.D.; *Gas Sep. Purif.* **1996**, *10*, 103.
- (11) Lu, G.Q. *Environ. Tech.* **1995**, *16*, 495.
- (12) Bagreev, A.; Locke, D.C.; Bandosz, T. J. *Carbon* **2001**, *39*, 1971.
- (13) Bandosz, T.J.; Bagreev, A.; Adib, F.; Turk, A. *Environ. Sci. Technol.* **2000**, *34*, 1069.
- (14) Adib, F.; Bagreev, A.; Bandosz, T.J. *Environ. Sci. Technol.* **2000**, *34*, 686.
- (15) Bagreev, A.; Bashkova, S.; Locke, D.C.; Bandosz, T.J. *Environ. Sci. Technol.* **2001**, *35*, 1537.
- (16) Bashkova, S.; Bagreev, A. Bandosz, T. J. *Environ. Sci. Technol.* **2002**, *18*, 1257.
- (17) Olivier, J.P. *J. Porous Materials***1995**, *2*, 9.
- (18) Adib, F.; Bagreev, A.; Bandosz, T.J. *J. Coll. Interface Sci.* **1999**, *214*, 407.
- (19) Adib, F.; Bagreev, A.; Bandosz, T.J. *J. Coll. Interface Sci.* **1999**, *216*, 360.
- (20) Katoh, H.; Kuniyoshi, I.; Hirai, M.; Shoda, M. *Appl. Cat. B: Environ.* **1995**, *6*, 255.

SIZE AND CHEMICAL CHARACTERISTICS OF FINE PARTICULATE EMISSIONS FROM OIL AND COAL-FIRED PILOT SCALE BOILERS

S. Win Lee, Ian He, Ted Herage and Bart Young

CANMET Energy Technology Centre
Natural Resources Canada
Ottawa, Canada, K1A 1M2

Introduction

The Canada Wide Standards for particulate matter (PM) was proposed in Canada in 2000, soon after the publication of the new US National Ambient Air Quality Standards in 1997^{1,2}. Subsequently, increased research activities were noted in the following years in addressing the apparent knowledge gaps related to fine PM emissions. Measuring PM_{2.5} and PM₁₀ emissions from combustion sources began to replace the traditional means of monitoring and reporting of total suspended particulates. Identification and quantification of PM from regional point sources are critical in controlling the PM emissions effectively at source as well as in apportioning the ambient PM concentrations to the contributing local sources. A new methodology was developed to determine fine PM emissions under plume-simulating conditions that are comparable to ambient PM characteristics. The method, unlike traditional high temperature measurement methods, applies initial cooling of the flue gas by diluting with clean air inside an inert tunnel to mimic plume conditions. The source dilution approach allows for atmospheric transformation processes for the PM and thus provides ambient-comparable source signature profiles for source apportionment modeling. At present, fine PM data from industrial sources are limited and often not representative of reality, being derived from high temperature source measurement techniques.

Research is being co-sponsored by two Canadian utilities, Environment Canada with the objective of examining source PM characteristics from the electric power generation sector. Two prototype samplers have been developed for the combustion units having low stack velocities (<5 m/s) and medium velocities (<10 m/s). The larger sampler is being retrofitted for field measurement on utility-scale boilers. The basic sampling protocol involves dilution of flue gas with purified air by 20 to 40 times inside a dilution chamber maintained at a 40% relative humidity (RH) to allow for cooling and simulation of atmospheric transformation processes. Portions of the diluted gas are withdrawn, while maintaining isokinetic sampling, through selected cyclone and impactor inlets and filter packs to collect the PM fractions. The method provides mass concentrations of PM_{2.5}, PM₁₀ and total PM and their size and chemical composition information. To date, fine PM emissions from the combustion of No. 2 and No. 4 heating fuels and pulverized coal have been determined and characterized using the two samplers. The paper summarizes the preliminary size and chemical characteristic data from the combustion of three experimental fuels.

Experimental

Fuels and Combustion Systems. A commercial No. 2 type, petroleum distillate oil was fired in a residential scale, 30 kW hot water boiler, Utica boiler Model Starfire 3. The ultimate analysis of the heating fuel showed 86.7% carbon, 13.5% hydrogen, 0.2% sulphur and 0.07% nitrogen, by mass. A larger oil-fired unit, 130 kW input capacity Weil-McLain Model 478, was used for burning the No. 4 type residual fuel oil. The fuel has 86.5% carbon, 12% hydrogen, 0.7% sulphur and 0.02% nitrogen. A western Canadian sub-bituminous coal blend was supplied by a utility for the combustion

experiments on a 0.7 MW_{th} pilot-scale research boiler. This boiler, a smaller model of a full-scale boiler, with its unique burner configurations can provide time-temperature profiles and typical ash behaviour of full-scale units. The coal blend has 9.6% moisture, 11.3% ash, 32.2% volatile matter and 56.5 fixed carbon. The ultimate analysis showed, 69% carbon, 4% hydrogen, 0.9% nitrogen and 0.2% sulphur. These combustion systems are fully equipped with fuel conditioning systems, continuous emission analyzers, temperature and pressure measurement devices and computer controlled data monitoring systems.

Combustion and Emission Measurement Procedures. The preparation of test facilities and experimental procedures for the combustion units have been reported elsewhere³⁻⁵. Normally the protocols require initial pre-warming of the units and calibration of the analyzers, followed by continuous monitoring of gaseous concentrations O₂, CO₂, CO, NO_x and SO₂ in the flue gas. The fine PM measurement was performed using the source dilution samplers when the experimental conditions were stabilized. An outline sketch of the source dilution sampler is shown in **Figure 1**. The sampling procedures for the units have been optimized and reported in previous publications⁴⁻⁶.

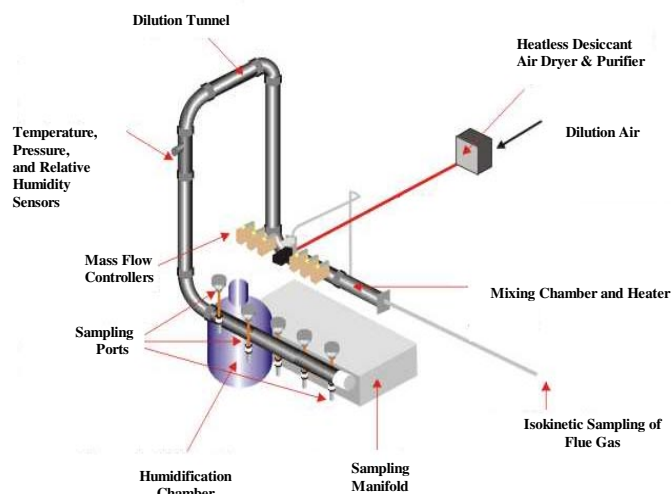


Figure 1. Source dilution fine PM measurement system.

PM Characterization Methods. The characterization protocol for the PM fractions has been published elsewhere⁶. Attention was given to ensure that the analytical techniques applied are comparable to those used in the analyses of ambient PM samples. The CCSEM (computer controlled scanning electron microscopy) was replaced with TEM (transmission electron microscopy) for examining size characteristics of the PM from No. 2 fuel combustion due to their extremely small size.

Results and Discussion

Size Distribution and Morphology. Typical CCSEM particle size analysis provides PM distribution expressed in terms of volume, corrected aerodynamic mass and number. A sample illustration for the No. 4 fuel is shown in **Figure 2**. Results from the multiple runs using five No.4 fuel blends, although not reported here, showed that this residual type fuel emits particles mostly made up of PM₁₀, about 85-90%. These particles are mainly carbon rich with sulphur being the second most abundant element detected. Coal fly ash samples showed

over 90% of PM₁₀, while the particles are Al and Si rich. In both types the presence of other trace elements such as V, Ni, Fe, Ca, Na and Ni are found although coal ash contains significantly higher mineral contents than the oil PM. However, the PM from the combustion of No. 2 fuel is predominantly in the 0.05µm range, thus requiring TEM analysis. The particles are mostly carbon and exist in the form of branched chain agglomerates and clusters. No measurable amounts of mineral matter are detected.

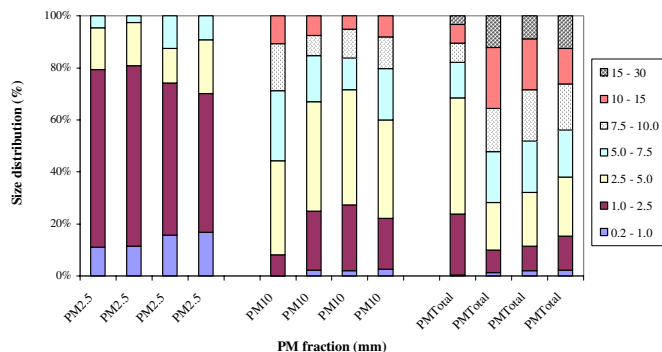


Figure 2. PM Size distribution from No. 4 fuel oil combustion. 0.7% sulphur, 40% RH, 26x dilution

PM Mass Concentrations. Filterable PM mass data is determined by gravimetric analysis using Teflon filters that are pre-conditioned in a control chamber maintained at 40% RH. Results are expressed in terms of particle mass in milligram per cubic metre of dry flue gas at standard temperature and pressure. As expected, the total PM fraction shows the highest mass, followed by PM₁₀ and PM_{2.5} in descending order for the test fuels, with the exception of No. 2 fuel. The mass data for No. 4 fuel revealed that the particles contain about 75-90% PM₁₀ and 50-70% PM_{2.5}. Preliminary research data for the sub-bituminous coal showed that fly ash samples at the ESP exit, contain about 80-85% PM₁₀ and 30-50% PM_{2.5}. However, the No. 2 fuel PM mass concentrations are similar for all size fractions, suggesting that they are all in the PM_{2.5} range. The reproducibility of results for No. 4 fuel combustion is very good, with relative standard deviation of less than 5%. Emission sampling for pulverized coal and No. 2 fuel are inherently more difficult due to the sticky nature of fly ash and the very low concentrations from clean-burning distillate fuels. The reproducibility for these results is about 5-15%.

Chemical Species and Simple PM Mass balance. The PM from stationary combustion sources generally contains carbonaceous species, mineral matter and condensed acidic compounds such as sulphates and nitrates. Replicate samples of filterable PM fractions are analysed for trace elements, organic carbons, elemental carbons and sulphates using the established analytical scheme⁶. The results showed up to 86% of mineral matter in the fly ash with about 5% carbons and 3% soluble sulphates. Trace elements are preferentially enriched in the PM_{2.5} fraction. Trace elements, carbons and soluble sulphates exist in the order of 10-12%, 50-90% and 20-40% respectively for the No. 4 fuel. The No. 2 fuel generated PM contains about 20-30% carbons, 40-50% sulphates and 20-30% water that exists as water of hydration associated with sulphate. It should be noted that these percentages would change when fuel sulphur content is varied. The PM speciated mass data for each fuel was reconstructed following simple assumptions used in ambient PM monitoring. The data in Table 1 indicates comparable mass concentrations between gravimetric analysis and the composite data. This information is necessary in

developing PM source characteristic profiles for mathematical source apportionment modelling.

Table 1. PM mass balance of experimental fuels (mg/m³) 40x dilution, 40% R.H.

Fuel		PM _{2.5}	PM ₁₀	PM _{Total}
0.05% S Diesel 30 kW Boiler	Metal as oxides	0.03	0.02	0.02
	Organic carbon	0.71	0.71	0.68
	Elemental carbon	1.00	1.03	1.03
	Sulphate & Hydration	0.57	0.51	0.51
	By composition analysis	2.31	2.27	2.24
	By gravimetry	1.93	2.09	2.09
0.2% S #2 Fuel 30 kW Boiler	Metal as oxides	0.10	0.09	0.09
	Organic carbon	1.24	1.27	1.12
	Elemental carbon	0.69	0.73	0.76
	Sulphate & Hydration	4.69	4.90	5.76
	By composition analysis	6.72	6.99	8.06
	By gravimetry	9.76	9.86	9.80
0.7% S #4 Fuel 130 kW Boiler	Metal as oxides	2.77	4.89	5.50
	Organic carbon	13.10	14.81	12.44
	Elemental carbon	4.22	11.65	14.27
	Sulphate & Hydration	10.10	10.73	12.73
	By composition analysis	30.19	42.08	44.94
	By gravimetry	34.23	43.54	50.33
0.23% S Bituminous C Coal 0.7 MW Boiler	Metal as oxides	31.00	86.00	99.00
	Organic carbon	3.00	4.00	4.00
	Elemental carbon	0.00	0.00	0.00
	Sulphate & Hydration	2.00	2.00	2.00
	By composition analysis	36.00	92.00	106.00
	By gravimetry	38.00	77.00	91.00

References

- (1) Canada Wide Standards. For PM and Ozone; *Canada Gazette*, Part I, Vol 134, No. 22, May 27, 2000, pp 1343-1645.
- (2) *Fed. Regist.* 62 FR38652, July 1997.
- (3) Lee, S. Win; Whaley, H.; Pomalis, R.; Wong, J.K.L. *ASME, EC-Vol. 5. 1997*, 97-105.
- (4) Lee, S. Win; Kan, B.; Pomalis, R. In: *Proceedings of 5th International Conference on Clean Air and Combustion Technology*, Lisbon, Portugal, July 12-15, 1999.
- (5) Lee, S. Win; Pomalis, R.; Kan, Betty. *Fuel Process. Technol.* **2000**, 65-66, 189-202.
- (6) Lee, S. Win. *J. Air & Waste Manage. Assoc.* **2001**, 51, 1568-1578.

SOURCE APPORTIONMENT OF PM_{2.5} IN BEIJING

Kebin He^a, Qiang Zhang^a, Yongliang Ma^a, Fumo Yang^a, Steven Cadle^b, Tai Chan^b, Patricia Mulawa^b, Chak K. Chan^c, Xiaohong Yao^c

^aDepartment of Environmental Science and Engineering
Tsinghua University, Beijing 100084, PRC

^bGM Research & Development
480-106-269, Warren, MI, 48090-9055, USA

^cDepartment of Chemical Engineering, The Hong Kong University
of Science & Technology, Clear Water Bay, Hong Kong, PRC

Introduction

Recently, the air pollution becomes more serious in Beijing. Fine particulates pollution, which significantly impairs human health, exceeds the air quality standards greatly. Since the end of 1998, the municipal government of Beijing began to implement a series of emergent measures by phases to keep urban air pollution from becoming more serious. The effect of the four phases indicated that lowering emissions from local sources was effective for SO₂ and NO_x emission reduction, but was not very effective for fine particulates. According to the results of current control measures and future control plans, it is difficult to reduce fine particulates concentration to meet the standards. To determine the source of ambient PM_{2.5} is the key issue of fine particulates pollution control.

One week integrated PM_{2.5} samples were collected continuously at two sampling sites for over one year starting in July 1999. Samples were collected simultaneously at two sites in Beijing: one located at Chegongzhuang in a downtown area, and the other located one on the campus of Tsinghua University in a residential area. This paper examines the source contribution of ambient PM_{2.5} by enrichment factor model and receptor model.

Experimental

A low-flow rate sampler with a 0.4l/min flow-rate was deployed at each site. X-ray fluorescence (XRF), ion chromatography (IC), and thermal/optical reflectance (TOR) were used to analyze 40 elements (from Na to U), water-soluble ions, and organic and elemental carbon (OC and EC), respectively. The detail information about Sampling system, chemical analysis, and quality control for this study has been introduced elsewhere¹.

It is considered that the element could be determined when the element concentration value is larger than double of its uncertainty value. Under this rule, fourteen elements (including Na, Mg, Al, Si, S, Cl, K, Ca, Fe, Cu, Zn, Se, Br, Pb), five ions (NH⁴⁺, K⁺, Cl⁻, NO₃⁻, SO₄²⁻), EC and OC were used for source apportionment.

Results and Discussion

Enrichment factor of elements. Enrichment factor model is a good pollution indicator of human activity. Enrichment factor is given by the following equation:

$$EF = \frac{(C_i / C_n)_{Environment}}{(C_i / C_n)_{Background}}$$

where C_i is the concentration of element i,

and C_n is the concentration of background element.

Aluminium was used as the background element in this paper because its soil concentration was stable and ambient concentration was little impacted with human activity. The element background concentration in the soil of Beijing was taken as the concentration of

background element². The values are: Na 13.1mg/g, Mg 12.7mg/g, Al 69.9mg/g, Si 330mg/g, S 850ug/g, Cl 1000ug/g, K 19.3mg/g, Ca 15.2mg/g, Fe 29.7mg/g, Cu 23.6ug/g, Zn 102.6ug/g, Se 0.25ug/g, Br 3.05ug/g and Pb 25.4ug/g.

According to the enrichment factors, these 14 kinds of elements can be classified into two groups. One group is crustal elements, including Na, Mg, Al, Si, K, Ca, and Fe. The enrichment factors of Na, Mg, Al, Si, Ca, and Fe at the two sites were all less than 10, which is because that these elements came from crustal dust and hadn't been influenced greatly by human activities. The enrichment factor of K was a little larger than 10, due to the contribution of biomass fuel combustion around Beijing. The other group is pollutant element, including S, Cl, Cu, Zn, Se, Br, and Pb. The enrichment factors of these 7 elements were all greatly larger than 10, indicating that they were closely related with human activities. The enrichment factors of S, Zn, Se, Br, and Pb were even over 500. S mainly came from coal smoke and the conversion of SO₂ to sulfate. Zn was the trace element of municipal garbage. Se and Br were trace elements of coal combustion and oil combustion, respectively. Pb was related with various process of combustion. As Beijing now uses unleaded gasoline, Pb may come from the coal and vegetation combustion. High enrichment level of these elements showed that the anthropogenic PM_{2.5} in Beijing was caused by the combustion of fossil fuel.

Table 1: Enrichment factors of elements in PM_{2.5}

Element	Tsinghua		Chegongzhuang	
	Number	Average	Number	Average
Na	36	3.2	36	4.3
Mg	34	1.5	36	1.7
Al	36	1	36	1
Si	36	0.7	36	0.7
S	36	803.2	36	793.3
Cl	36	372.2	36	313.7
K	36	15.6	36	14.9
Ca	36	7.3	36	7.2
Fe	36	3.7	36	3.6
Cu	36	176.4	36	169.8
Zn	36	583.8	36	498.7
Se	36	4049.2	36	4133.6
Br	36	832.7	36	596.8
Pb	36	1348.6	36	1270.9

Apparent seasonal variety of the enrichment factors at the two sample sites can be observed. Higher enrichment level occurred at the autumn and winter and lower enrichment level occurred at the spring. At the Tsinghua and Chegongzhuang sample sites, the enrichment factors of the crustal elements in winter were 49.7% and 43.1% respectively higher than those in spring. This seasonal variety was more obvious for pollutant elements. The enrichment factors of the 7 pollutant elements at the Tsinghua and Chegongzhuang sites in winter were 192.5% and 171.9% higher respectively than those in spring (as shown in **Figure 1**). According to Figure 1, except for Br, the enrichment factors of the other six elements reached peak value at winter, second highest value at autumn and lowest value at spring.

The significant seasonal difference of the pollutant elements' enrichment factors is due to the increased fossil fuel combusted in the heating periods. Besides, poor meteorological conditions in winter and autumn, such as dry climate and poor atmospheric dispersion conditions, is also an important reason that causes the seasonal difference of the enrichment factors.

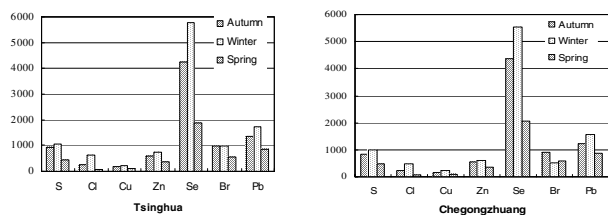


Figure 1: Seasonal variation of enrichment factors on pollutant elements.

Figure 2 shows that the enrichment factors of the two samples didn't vary a lot with difference of most of the enrichment level within 10%, which is because that small particle diameter of $PM_{2.5}$ can make itself stay in the atmosphere for a long time and mix evenly in a definite spatial range.

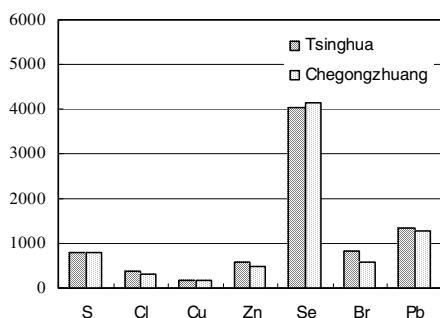


Figure 2: Spatial variation of enrichment factors on pollutant elements.

Source apportionment by receptor model

The software CMB 8.0 was used to estimate the contribution of the sources to the $PM_{2.5}$ mass of each sample in this paper. The CMB 8.0 software provides several indicators of the model results. In this study, most of main indicators were matched the model requirement.

The chemical mass balance model was used for source apportionment in this study. This method requires the detail chemical profiles of each emission source. In this study, the $PM_{2.5}$ emission source was divided into the following types: road dust, cement dust, residential boiler, industrial boiler, vehicle exhaust and secondary ammonium. The composition of road dust, residential boiler and industrial boiler were based on the study of Chen et al.³ The cement dust profiles was adopted (SPECIATE profile No. 27204) from the EPA $PM_{2.5}$ source profiles database. The composition of vehicle exhaust was adopted from the draft result of the Beijing Air Pollution Control Project.

On average, the major contributors of $PM_{2.5}$ samples at two sites are shown in Figure 3. The average concentration of $PM_{2.5}$ was $146\mu g/m^3$ and $138\mu g/m^3$ in Tsinghua and Chegongzhuang respectively. The total contribution of the source accounts to $115.6\mu g/m^3$ and $114.5\mu g/m^3$, respectively. Coal boiler (residential boiler and industrial boiler) is the largest contributor of $PM_{2.5}$ at both

sites, followed by secondary ammonium, road dust, vehicle exhaust and cement dust. About 20% of $PM_{2.5}$ mass was not determined by CMB. The undetermined sources maybe include biomass burning and sea salt, etc. The Source contribution to $PM_{2.5}$ at two sites was very similar, which indicates that the ambient $PM_{2.5}$ of those two sites has same sources. The coal consumption of residential boilers occupied 10%-15% of industrial boiler⁴ but its contribution to $PM_{2.5}$ was similar with the industrial boilers. The major reason is from the lower fuel efficiency and higher PM emission factor of residential boilers.

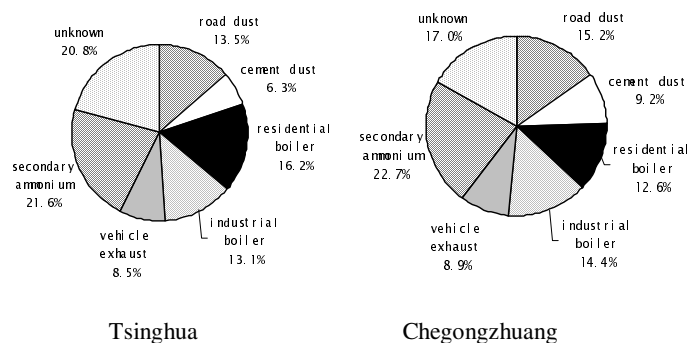


Figure 3: Average source contribution to $PM_{2.5}$ at two sites.

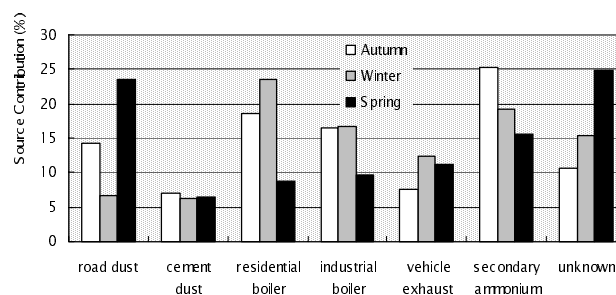


Figure 4: Seasonal variation of $PM_{2.5}$ source contribution at Tsinghua site.

Figure 4 shows the seasonal variation of $PM_{2.5}$ source contribution at Tsinghua site. The similar result was found at Chegongzhuang site. The road dust contribution to $PM_{2.5}$ reached the peak in spring because of the dust storm. The contribution from coal boilers reached the peak in the winter due to the heating system working.

Acknowledgment

This work was supported by GM Research and Development Centers.

References

1. He, K.; Yang, F.; Ma, Y.; Zhang, Q.; Yao, X.; Chan, K. C.; Cadle, S.; Chan, T.; Mulawa, P., *Atmospheric Environment*. **2001**. 35: 4959-4970.
2. China Environmental Monitoring Center, Chinese soil element background content, Chinese Environment Science Press, 1990.
3. Zongliang Chen, Su Ge, Jin Zhang, *Environment Science Research*, 1994, Vol.7, Issue 7: 1-9.
4. China National Bureau of Statistics, *China Energy Statistics Yearbook 1991-1996*, Chinese Statistics Press, 1997.